Deletion of Glycogen Synthase Kinase-3β in D_2 Receptor-Positive Neurons Ameliorates Cognitive Impairment via *N*-Methyl-D-Aspartate Receptor-Dependent Synaptic Plasticity

Supplementary Information

Supplemental Methods and Materials

Animals

The GSK-3β$^{flox/flox}$ Drd1Cre (D1R-GSK-3β$^{-/-}$) mouse and GSK-3β$^{flox/flox}$ Drd2Cre (D2R-GSK-3β$^{-/-}$) mouse were generated at Duke University as described previously (1). Briefly, The D1RCre and D2RCre mice were backcrossed onto a C57BL6/J background for at least five generations and then crossed with the GSK-3β$^{flox/flox}$ mouse (mixed BL6/129 background). Their offspring, including D1R-GSK-3β$^{-/-}$, D2R-GSK-3β$^{-/-}$ and their littermate controls (D1R-GSK-3β$^{+/+}$, D2R-GSK-3β$^{+/+}$) were used for experiments. All data were obtained from young adult mice (P60-P90, both male and female) with 140 D2R mice, 24 D1R mice, and 38 DISC1 strains used.

Transgenic mice expressing a Myc peptide-tagged mutant (truncated) human DISC1 gene under the control of tetracycline operator (tetO) (Tg(tetO-DISC1*)1001Plet/J, C57BL/6J background) was kindly gifted by Dr. Mikhail Pletnikov of Johns Hopkins University. This single-transgenic mutant hDISC1 mouse was bred with an activator mouse line (B6;CBA-Tg(Camk2a-tTA)1Mmay/J, Jackson Laboratory) to generate double-transgenic mutant hDISC1 mice for experiments. Male and female mice were used in equal number in each group. All data were obtained from young adult mice (P60-P90). The animals were treated in accordance with the guidelines of the National Institutes of Health and the experimental protocols were approved by the Institutional Animal Care and Use Committee at Drexel University College of Medicine.

All transgenic pups were weaned at P18-21. Tail tissues were collected for genotyping and primers are enlisted in the Key Resources Table.

Immunostaining

To validate the Cre line, D2R-GSK-3β-/- mice were crossed with Cre-dependent tdTomato$^{+/+}$ mice [B6.Cg-Gt(ROSA)26Sortm1.3(CAG-tdTomato,-EGFP)Pjen/J, Jackson Laboratory], allowing visual identification of D2R+ neurons. Immunostaining of GSK-3β was performed as described in the previous report (1). Briefly, Cortical sections containing mPFC were blocked with 5% goat normal serum diluted in 3% Triton-PB for 1 h at room temperature. Anti-GSK3β (1:250; Transduction Laboratories BD 610202; RRID: AB_397601) were applied and detected with fluorescent secondary antibodies. The sections were mounted with UltraCruz™ mounting medium and were then mounted, sealed, and imaged on a Zeiss Axiovert 200 M inverted microscope with Axiovision software (Zeiss Microscopy).

Electrophysiological Recording

Whole-cell patch-clamp recording: The detailed procedure can be found in our previous studies (2). Briefly, mice were deeply anesthetized with Euthasol (0.2 ml/kg; Virbac AH), and the brains were immediately removed and placed in ice-cold (4°C) sucrose-containing solution (in mM: 2.5 KCl, 1.25 NaH_2PO_4, 26 $NaHCO_3$, 0.5 $CaCl_2$, 7.0 $MgSO_4$, 213 sucrose, pH 7.4) buffered with 95% O_2 and 5% CO_2. The blocks of neocortex containing medial PFC (*PrL*) (Paxinos and Watson, 2005) were trimmed and sectioned using a Leica VT1200s Vibratome (Leica Microsystems). The horizontal brain slices at a thickness of 300 μm were incubated in oxygenated Ringer's solution (in mM): 128 NaCl, 2.5 KCl, 1.25 NaH_2PO_4, 2 $CaCl_2$, 1 $MgSO_4$, 26 $NaHCO_3$, and 10 dextrose, pH 7.4) at 35°C for 1 h. The PFC-containing slices were then incubated at room temperature until they were transferred to a submerged recording chamber. Whole-cell patch-clamp recordings were conducted from layer V pyramidal neurons through an upright Zeiss Axioskop 2 microscope (Carl Zeiss) equipped with infrared-differential interference contrast

optics and a digital video camera system. The recordings were conducted at ~35°C. The resistance of the recording pipette (1.2 mm borosilicate glass; Warner Instruments) was 5-7 MΩ. The recording pipettes were filled with a K^+-based intracellular solution to record membrane properties in a current-clamp mode in response to step currents from −300 to +400 pA with 50 pA increments.

In voltage clamp mode, to record AMPAR-mediated spontaneous (AMPAR-sEPSCs) and miniature excitatory postsynaptic currents (AMPAR-mEPSCs), the membrane potential was held at -60 mV with Cs+-based intracellular solution in the presence of APV (50 μM, Tocris) and picrotoxin (50 μM, Tocris) with (mEPSCs) or without tetrodotoxin (TTX, 1μM, Hello bio) (sEPSCs). To record NMDAR-sEPSCs and NMDAR-mEPSCs, the membrane potential was held at +60 mV in the presence of CNQX (20 μM, Tocris) and picrotoxin (50 μM, Tocris) with (mEPSCs) or without tetrodotoxin (TTX) (sEPSCs). Evoked AMPAR-mediated currents and NMDAR-mediated currents were elicited by stimulating layer II/III with a bipolar electrode placed ~300 μm from the target neurons (1 or 10 pulses at 20 Hz; 0.1 ms, 10–100 μA, 0.1 Hz). For NMDA/AMPA ratio, NMDAR-mediated current was measured at 50 ms after the peak amplitude in evoked EPSCs recorded at +60 mV in the presence of picrotoxin (50 μM, Tocris). This analysis can rule out the potential contribution of AMPAR-mediated current, which usually returns to baseline within 20 ms. For input-output curves, we recorded evoked NMDAR-EPSCs from each cell with three incremental intensities of stimulation in the presence of CNQX (20 μM) and picrotoxin (50 μM). To evaluate the presence of NR2A and NR2B, we recorded evoked NMDAR-EPSCs before and after bath application of selective NR2B blocker Ro 25-6981 for 5 minutes. *Extracellular recording:* For long-term potentiation (LTP) and long-term depression (LTD), experiments were conducted in current clamp mode. Slices were prepared as described above. The stimulating electrode was placed in layer II/III and a low-resistance (0.5–1 MOhm) recording glass

pipette containing Ringer's solution was placed in layer V of mPFC. For baseline recording, the stimulus intensity was set to elicit a field potential of ~0.5 mV peak amplitude and recorded for 15 min with a stimulus every 15 s. Responses were monitored online and only those recordings with stable baselines proceeded to LTP or LTD induction. To induce LTP, layer II/III was stimulated with six trains of 100 pulses at 100 Hz, with an inter-train interval of 30 s. To induce LTD, low-frequency stimulation (900 pulses at 1 Hz) was used. Thereafter, stimulation was given every 15 s for 45 min until the recording was suspended. The slope of the field potential was measured and data points for each minute were averaged.

Data analysis: All experiments were conducted with Axon MultiClamp 700B amplifier (Molecular Devices), data were acquired using pCLAMP 9.2 software and analyzed using Clampfit 9.2 (Molecular Devices). A typical s/mEPSC was selected to create a sample template for event detection within a 5-min data period. The frequency and amplitude of the individual events were examined. A representative evoked EPSC was obtained by averaging 30 traces and the amplitude was measured from the onset to the peak. For LTP/LTD recordings, the EPSP slope was measured relative to the normalized pre-induction baseline and data points for each minute were averaged. The magnitude of LTP and LTD were determined by comparing the average responses in the first and last 5 min of the 45-min recording after tetanus stimulation to the average baseline response.

Pharmacological treatment: At postnatal day 25 (P25), mutant hDISC1 mice and their littermate controls were treated with GSK-3β antagonist SB216763 (2 mg/kg/day, Tocris Bioscience) or vehicle (saline). A separate group of mutant hDISC1 mice and littermate controls were treated at P25 with either TAT-D2pep [K211-T225] (KIYIVLRRRRKRVNT) (10 mM, Biomatik) or scrambled control TAT-peptide (D2pep-sc) (VLRKTRIRRYKIRNV) (10 mM,

Biomatik). The treatments were delivered intraperitoneally once a day (8:00 AM – 10:00 AM) for 5 consecutive days (P25–P30). No further treatment was administered until adulthood when animals were used for electrophysiological experiments.

Viral microinjection

GSK-3β$^{flox/flox}$ mice at P25 were used for all surgeries. All mice received a bilateral viral injection into the mPFC with the assistance of a David Kopf Stereotaxic Instrument (model 900, David Kopf Instruments, Tujunga, CA). Briefly, anesthesia was induced with 3% isoflurane in O_2 by inhalation and maintained with 1.5–2% isoflurane throughout the surgery. The stereotaxic coordinates for the mPFC were +2.05 mm from bregma, ±0.35 mm lateral from the midline, and −1.50 mm ventral from the dura. Adeno-associated virus (AAV)-expressing Cre (AAV8-hSyn-Cre-mCherry, UNC vector core) or control virus (AAV8-hSyn-GFP)(3, 4) was injected by a syringe pump at a rate of 2.2 μl/hour, with 500 nl volume injected per site in each mouse. After surgery, animals recovered for five weeks prior to electrophysiological recording.

Western blotting

Whole cell protein: mPFC was dissected, homogenized in ice-cold lysis buffer [in mM: 20 Tris-HCl, pH 7.4, 150 NaCl, 1 EDTA, 1 sodium orthovanadate, 0.1 phenylmethylsulfonyl fluoride, 50 sodium fluoride, 10 sodium pyrophosphate, 20 glycerophosphate, with 0.1% sodium dodecyl sulfate (m/V), 0.01% Triton X (V/V), 0.25% sodium deoxycholate (m/V), 1 μg/ml leupeptin, 1 μg/ml aprotinin and 1 μg/ml pepstatin]. Homogenates were incubated on ice for 30 min and then centrifuged at 13,000g for 5 min. After measurement of protein concentration by bicinchoninic acid (BCA) protein assay, 10-15 μg of protein were resolved by electrophoresis on 7.5% SDS-PAGE gels and transferred onto polyvinylidene difluoride membranes (PVDF; Millipore). The membranes were blocked in 5% nonfat milk in Tris-buffered saline for 1 h and were incubated

with the following primary antibodies overnight at 4°C: anti-NR1 antibody (1:1000, Millipore, #32-0500，RRID: AB_2533060, Billerica, MA), anti-NR2A antibody (1:1000, Millipore, #04-901 ； RRID:AB_1163481), anti-NR2B antibody (1:1000, Millipore, #05-920 ； RRID: AB_417391), anti-GluR1 antibody (1:2000, Millipore #MAB2263; RRID: AB_11212678), anti-GluR2 antibody (1:2000, Millipore #MABN71; RRID: AB_10806492); anti-GSK-3β antibody (1:5,000; Cell Signaling Technology, 9315; RRID:AB_490890; Danvers, MA), anti-GSK-3β ser9 antibody (1:2,000; Cell Signaling Technology, 9336S; RRID:AB_ 331405), anti-GSK Tyr279/216 antibody (1:2000, Millipore #MAB05413; RRID: AB_ 309721) and β-actin (1:100,000; Sigma-Aldrich, A5316; RRID: AB_476743； St Louis, MO, USA). After several washes with Tris-buffered saline with Tween, the blots were incubated in horseradish peroxidase-conjugated goat anti-mouse or anti-rabit IgG secondary antibody (Jackson ImmunoResearch Laboratories) at 1:4000 for 1 h.

Histone protein: mPFC tissue collection and protein assay were performed as described above. The Epiquik Total Histone Extraction Kit (OP-0006, EpiGentek, Farmingdale, NY) was used to isolate the histone fraction. 15 μg of histone-enriched protein was loaded on a 15% SDS-PAGE gel. After electrophoresis, blots were transferred to pore size 0.20 μm PVDF membranes. Membranes were blocked with 5% nonfat milk and separately probed with the following primary antibodies: anti-HDAC2 (1:5000, Abcam, ab12169；RRID: AB_2118547; Cambridge, UK), anti-HDAC4 (1:5000, Abcam, ab123513；RRID:AB_11000944), anti-H3K9ac (1:5000, Abcam, ab10812；RRID: AB_297491), anti-H3K18ac (1:5000, Abcam, ab1191；RRID: AB_298692), anti-H3K27ac (1:5000, Abcam, ab4729 ； RRID: AB_2118291) and anti-total histone H3 (1:100,000, Novus, NB500-171； RRID: AB_10001790; Littleton, CO) was used as a loading

control. Blots were incubated with horseradish peroxidase-coupled anti-rabbit or anti-mouse IgG secondary antibody (1:5000, Jackson ImmunoResearch Laboratory) for 1 h.

Data collection and analysis: The immunopositive protein bands were detected with the ECL Western Blotting System (GE Healthcare Life Sciences). After exposure of the membranes to Kodak Biomax film (Eastman Kodak), the band densities were measured with NIH ImageJ software. Final data were normalized to the levels of β-actin (whole cell protein) or H3 (histone protein). To minimize the interblot variability, each tissue sample from an animal was analyzed four times from at least two different gels. The mean protein density for each animal was calculated from all the replicates, and the results are presented as mean ± SEM. The N is the number of animals in each group. Significance was determined by the Student *t*-test or ANOVA.

BS3 cross-link assay for AMPAR subunits

Bis (sulfosuccinimidyl) suberate (BS3) cross-linking assay was performed as described previously (2, 5). PFC slices were collected as described in Electrophysiological Recording. After incubation of PFC with oxygenated Ringer's solution at 35°C for 30 minutes, the slices were transferred into the plates containing 1 mM BS3 (Pierce Biotechnology) and incubated for 30 min at room temperature with gentle agitation. The slices were then washed three times with ACSF containing 20 mM Tris, pH 7.6, to quench the remaining BS3. Proteins were extracted from homogenized slices and prepared for Western blot analysis.

Chromatin immunoprecipitation-qPCR assay

mPFC tissue was collected as described above and pooled for chromatin immunoprecipitation (ChIP) assay. The ChIP assays were performed with the truChIP^{TM} Chromatin Shearing Kit (Covaris, PN 520237). Three separate reactions with 25 μg of sheared chromatin were carried out using: 1 μg HDAC2 antibody (Abcam, PN: ab7029), 1 μg H3K27ac

antibody (Abcam, PN: ab4729), and a mock reaction containing all reagents with IgG antibody as a control. The chromatin was immunoprecipitated using the EZ-Magna ChIP™ A-Chromatin Kit (Millipore; 17-408). The eluted material was purified using a QIAquick PCR kit (Qiagen; 28104) and was directly used for qPCR. Positive and negative control primer sets were purchased from Active Motif (71027, 71024). PCRs were performed in a 20-μL reaction containing purified chromatin DNA, 1 mM Power SYBR Green PCR Master Mix (Applied Biosystems; 4367659), and 10 mM of both forward and reverse primers, reported by Rodenas-Ruano, Chavez (6) (See Key_Resouces_Table). PCR was performed in triplicate using an ABI 7500 system (Applied Biosystems). ChIP-qPCR signals were calculated as a percentage of input. Data were obtained from 3 biological replicates (n=6 animals).

Golgi–Cox staining

Mice were anesthetized, decapitated and the forebrains were rapidly dissected and rinsed with double distilled water to remove blood from the surface. Golgi-Cox impregnation of brain tissue was conducted using the FD Rapid GolgiStain Kit (FD NeuroTechnologies, Inc., Ellicott City, MD). Briefly, tissue was immersed in G–C solution (a mixture of A and B solutions from a kit) for 2 weeks at room temperature. Following 14 days of impregnation, tissues were transferred to solution C and incubated for at least 2 days at 4°C before being sectioned. Forebrain area containing medial PFC was then embedded in Cryo-OCT compound (Fisher Scientific), blocked, and cut coronally at -20°C to -22°C (100 μm sections) on a cryostat microtome (Microm; Thermo Scientific, Wilmington, DE). After immediately mounting onto 0.3% gelatin-coated slides with solution C, slides were then immersed in a mixed buffer (solution D, solution E and distilled water) for 10 min. Slides were then washed and dehydrated with gradient ethanol series, cleared with xylene (three times for 4 min each), and coverslipped with Permount (Fisher Scientific). The

analysis was performed on marked Golgi impregnated brain sections containing the PFC from four mice per group, and nine to ten pyramidal neurons within layer II/III or layer V of mPFC were then measured for spine density as previously described (7, 8). Only neurons with clear cell bodies and primary dendrites that could be easily distinguished from neighboring cell bodies and their dendrites were selected for pictures and analysis. Dendritic spines were sampled from dendritic branches in the apical trunk at a distance of ~100-200 μm from the soma of pyramidal neurons in layers II-III or V. Spine density was counted and analyzed with reference to the length of the dendrite by Neurolucida Explorer (version 9) and the results were expressed as the average number of spines per 10 μm.

Attention set-shifting task

Transgenic mice were assigned to eight treatment groups: saline + D1R-GSK-3$\beta^{+/+}$, saline + D1R-GSK-3$\beta^{-/-}$, saline + D2R-GSK-3$\beta^{+/+}$, saline + D2R-GSK-3$\beta^{-/-}$, MK-801 + D1R-GSK-3$\beta^{+/+}$, MK-801 + D1R-GSK-3$\beta^{-/-}$, MK-801 + D2R-GSK-3$\beta^{+/+}$, MK-801 + D2R-GSK-3$\beta^{-/-}$. All mice were food-restricted to 85% of their free-feeding weight prior to any behavioral training. The injection procedure was identical for each animal. The set-shifting task was implemented as described previously (9). Briefly, the set-shifting task was carried out in a wooden cross maze that was painted white, with four 14.5 × 4.5 × 9.0 in. arms. Animals were habituated to the maze for two days and their turn bias was determined on the third day. On the fourth day, animals had to demonstrate learned response discrimination and on the fifth and final day, shift their responses based on a visual cue. On the test day (fifth day), the injection was given 30 min before training started. Different groups of mice received saline (0.9%, i.p.) or an NMDAR antagonist MK-801 (0.06 mg/kg dissolved in 0.9% saline, i.p.; Ascent Scientific, Bristol, UK). The dose of MK801 was in accordance with previous work (10) and our own studies (9, 11). In our preliminary studies,

we also tested a higher dose of MK-801 (0.1 mg/Kg) that was used for building set-shifting deficit model on rat [9]. However, the mice injected with this dose of MK-801 were unable to acquire the task and reach criterion. Hence, they could not normally perform the behavioral test due to the side-effects of increased locomotion. Data collected from the fifth day of the task were analyzed for the total number of trials to criterion and the number of probe trials required to reach criterion. For the shift to a visual cue, errors are scored as entries into arms that did not contain the visual cue and then further divided into 3 subcategories. Perseverative errors are when the mice continue to use the old strategy. Regressive or never-reinforced errors occur when the animal is unable to maintain the use of the new strategy. Student's unpaired *t*-tests or ANOVA followed by a simple effect test or t-tests were performed as appropriate to determine the statistical significance with Prism v5.0 (GraphPad Software) and IBM SPSS 19.0 Statistics. All data are presented as mean ± SEM.

Supplemental Results

Neither AMPAR-sEPSCs nor -mEPSCs were altered in D2R-GSK-3$\beta^{-/-}$ mice compared with their littermate controls (D2R-GSK-3$\beta^{+/+}$) (n=25, amplitude of sEPSCs: D2R-GSK-3$\beta^{+/+}$ 11.0±1.15 vs. D2R-GSK-3$\beta^{-/-}$ 10.8±0.88, $p > 0.05$; amplitude of mEPSCs: D2R-GSK-3$\beta^{+/+}$ 9.85±0.75 vs. D2R-GSK-3$\beta^{-/-}$ 8.58±0.45 $p > 0.05$; frequency of sEPSCs: D2R-GSK-3$\beta^{+/+}$ 1.48±0.39 vs. D2R-GSK-3$\beta^{-/-}$ 2.09±0.38, $p > 0.05$; frequency of mEPSCs: D2R-GSK-3$\beta^{+/+}$ 0.89±0.23 vs. D2R-GSK-3$\beta^{-/-}$ 1.09±0.22 $p > 0.05$; Figure 1A).

The amplitudes of both NMDAR-sEPSCs and NMDAR-mEPSCs were significantly increased in D2R-GSK-3β GSK-3$\beta^{-/-}$ mice (n=20 for each group, sEPSCs: D2R-GSK-3$\beta^{+/+}$ 11.9±1.10 vs. D2R-GSK-3$\beta^{-/-}$ 17.6±2.17, $*p < 0.05$; mEPSCs: D2R-GSK-3$\beta^{+/+}$ 12.0±1.48 vs. D2R-GSK-3$\beta^{-/-}$

18.2±1.30 *p < 0.05; Figure 1B), although the frequency was unaltered (n= 20 for each group, sEPSCs: D2R-GSK-3β$^{+/+}$ 0.81±0.17 vs D2R-GSK-3β$^{-/-}$ 0.62±0.09, p >0.05; mEPSCs: D2R-GSK-3β$^{+/+}$ 0.49±0.11 vs. D2R-GSK-3β$^{-/-}$ 0.38±0.07, p > 0.05; Figure 1B). The amplitudes of evoked NMDAR-EPSCs induced by a series of stimulus intensities were significantly increased in D2R-GSK-3β-/- mice vs. D2R-GSK-3β$^{+/+}$ mice (two-way ANOVA, n=11/group, genotypes: *p<0.05 F=6.05, stimulation intensity: ***p <0.01 F=18.5; Post-hoc tests: 6V D2R-GSK-3β$^{+/+}$ 91.19±32.4 vs. D2R-GSK-3β$^{-/-}$ 238.7±70.1, *p <0.05; 7V D2R-GSK-3β$^{+/+}$ 145.7±39.31 vs. D2R-GSK-3β$^{-/-}$ 435.61±20.6, *p <0.05; 8V D2R-GSK-3β$^{+/+}$ 214.5±53.53 vs. D2R-GSK-3β$^{-/-}$ 613.6±143.7 *p <0.05 Figure S2). D1R-GSK-3β-/- mice, no alteration of NMDAR-sEPSCs and NMDAR-mEPSCs was detected (n=16 for each group, amplitude of sEPSCs: D1R-GSK-3β+/+ 14.02±0.49 vs. D1R-GSK-3β-/- 15.00±0.85, p>0.05; amplitude of mEPSCs: D1R-GSK-3β$^{+/+}$ 14.00±0.05 vs. D1R-GSK-3β$^{-/-}$ 12.21±0.80 p>0.05; frequency of sEPSCs: D1R-GSK-3β$^{+/+}$ 0.82±0.07 vs. D1R-GSK-3β$^{-/-}$ 0.63±0.08, p >0.05; frequency of mEPSCs: D1R-GSK-3β$^{+/+}$ 0.74±0.11 vs. D2R-GSK-3β$^{-/-}$ 0.52±0.13 p >0.05; Figure S3).

We found that D2R-GSK-3β$^{-/-}$ mice exhibit larger NMDA/AMPA ratio of both the first EPSC and the second EPSC, compared with D2R-GSK-3β$^{+/+}$ mice (n=8 for each group, first pulse: D2R-GSK-3β$^{+/+}$ 0.85±0.22 vs. D2R-GSK-3β$^{-/-}$ 2.46±0.62; second pulse: D2R-GSK-3β$^{+/+}$ 0.69±0.14 vs. D2R-GSK-3β$^{-/-}$ 3.23±0.86; ** p <0.01 for all, Figure 1C).

The amplitudes of both AMPAR-EPSCs and NMDAR-EPSCs exhibited short-term depression in D2R-GSK-3β$^{+/+}$ mice and D2R-GSK-3β$^{-/-}$ mice. The amplitude of the first NMDAR-EPSC recorded from D2R-GSK-3β$^{-/-}$ mice was significantly increased (n=10 for each group, D2R-GSK-3β$^{+/+}$ 1.00±0.28 vs. D2R-GSK-3β$^{-/-}$ 2.14±0.22, **p < 0.01; Figure 1D upper left), however, the PPRs from the 2nd to 10th NMDAR-EPSCs between D2R-GSK-3β$^{+/+}$ mice and D2R-GSK-3β$^{-/-}$

mice were not altered ($p > 0.05$ for all; Figure 1D upper left). This finding suggests that the increased NMDAR-mediated currents were likely due to postsynaptic mechanisms. Furthermore, neither amplitude of the first AMPAR-EPSCs nor PPRs from the 2nd to 10th AMPAR-EPSCs showed significant differences between D2R-GSK-3$\beta^{+/+}$ mice and D2R-GSK-3$\beta^{-/-}$ mice (n=10 for each group, first amplitude: D2R-GSK-3$\beta^{+/+}$ 1.00±0.19 vs. D2R-GSK-3$\beta^{-/-}$ 1.28±0.15, $p>0.05$; PPRs: D2R-GSK-3$\beta^{+/+}$ vs. D2R-GSK-3β-/-, $p > 0.05$ for all; Figure 1D upper right). The charge transfer of NMDAR-EPSCs, but not AMPAR-EPSCs, was significantly increased in D2R-GSK-3$\beta^{-/-}$ mice vs. D2R-GSK-3$\beta^{+/+}$ mice (n=10 for each group, NMDAR-EPSC: D2R-GSK-3$\beta^{+/+}$ 353.9 ± 23.57 vs. D2R-GSK-3$\beta^{-/-}$ 501.7 ± 73.98, $^{**}p < 0.01$; AMPAR-EPSC: D2R-GSK-3$\beta^{+/+}$ 79.7 ± 12.4 vs. D2R-GSK-3$\beta^{-/-}$ 88.1 ± 25.6, $p > 0.05$, Figure 1D lower).

We found that the amplitude of NMDAR-mEPSCs were significantly increased (n=6 for each group, Cre virus group 14.0±1.99 vs. control virus group 20.8±1.65, $^{*}p < 0.05$; Figure S2) in fluorescence-labeled layer V pyramidal neurons, although the amplitude of sEPSCs and frequency of both sEPSCs and mEPSCs were unchanged (n=6 for each group, amplitude of sEPSC: Cre virus group 15.8±1.93 vs. control virus group 17.7±0.89; frequency of sEPSC: Cre virus group 1.25±2.90 vs. control virus group 0.82±0.22; frequency of mEPSC: Cre virus group 1.18±0.29 vs. control virus group 0.80±0.22; $p > 0.05$ for all; Figure S4).

As shown in Figure 1E, after a low dose (0.2 μM) of DA was applied for 10 min to layer V pyramidal cells in D2R-GSK-3$\beta^{+/+}$ mice, NMDAR-EPSCs were significantly increased (n=8, 1.32±0.11, $^{*}p < 0.05$; Figure 1E left) and this persisted for a further 10 min after DA washout (n= 8, 1.65±0.14, $^{**}p < 0.01$; Figure 1E left), whereas an intermediate dose (20 μM) of DA induced a slight increase in EPSC amplitude (n=8, 1.04±0.12, $p >0.05$; Figure 1E middle). A high dose (200 μM) of DA significantly decreased the amplitude of NMDAR-EPSCs (n= 8, 0.81±0.06, $^{*}p < 0.05$;

Figure 1E right). Surprisingly, the bidirectional effect of DA was significantly changed in D2R-GSK-3β$^{-/-}$ mice compared with their littermate controls; 0.2 μM DA robustly enhanced NMDAR-EPSC amplitude (n=8; 1.73±0.11 after DA application and 2.29±0.20 after wash-out, **p < 0.01 for both; D2R-GSK-3β$^{+/+}$ vs. D2R-GSK-3β$^{-/-}$ #p <0.05 for both, Figure 1E left), whereas the 200 μM DA induced-depressive effect on NMDAR-EPSC amplitude completely disappeared and even showed a slight increase (n= 8, 1.04±0.08, p > 0.05; Figure 1E right). The effect of 20 μM DA on NMDAR-EPSCs was, however, unchanged in D2R-GSK-3β$^{-/-}$ mice (n=8, 1.18±0.21, p > 0.05, Figure E middle).

The fEPSP slope significantly increased in D2R-GSK-3β$^{-/-}$ mice following the LTP induction protocol [n=10 for each group; normalized EPSP slope; compared with baseline, first 5 min post-tetanus: D2R-GSK-3β$^{+/+}$ 1.01±0.12 p >0.05, D2R-GSK-3β$^{-/-}$ 1.36±0.10, *p <0.05; last 5 min post-tetanus (30-35 min after high-frequency stimulation): D2R-GSK-3β$^{+/+}$ 0.96±0.14 p >0.05, D2R-GSK-3β$^{-/-}$ 1.26±0.10, *p <0.05; Figure 2A], suggesting that synaptic strength is potentiated in D2R-GSK-3β$^{-/-}$ mice. Next, we tested the cell-type specific effects of GSK-3β ablation on LTD. We used a low-frequency stimulation protocol (900 pulses at 1 Hz). The fEPSP slope significantly decreased in D2R-GSK-3β$^{+/+}$ mice, demonstrating that induction of LTD in the mPFC does not require DA. In contrast, LTD could not be induced in D2R-GSK-3β$^{-/-}$ mice (n=8 for each group; normalized EPSP slope; compared with baseline, first 5 min post-tetanus: D2R-GSK-3β$^{+/+}$ 0.60±0.14 *p <0.05, D2R-GSK-3β$^{-/-}$ 0.91±0.18, p >0.05; last 5 min post-tetanus (30-35 min after low-frequency stimulation): D2R-GSK-3β$^{+/+}$ 0.53±0.16, * p <0.05, D2R-GSK-3β$^{-/-}$ 1.10±0.26, p >0.05; Figure 2B).

The spine density on apical dendrites of layer V, but not layers II-III, pyramidal neurons in D2R-GSK-3β$^{-/-}$ mice was significantly increased (n=10 for each group; layer II-III: D2R-GSK-

$3\beta^{+/+}$ 3.09±0.13 vs. D2R-GSK-$3\beta^{-/-}$ 3.08±0.14, p >0.05; layer V: D2R-GSK-$3\beta^{+/+}$ 2.25±0.28 vs. D2R-GSK-$3\beta^{-/-}$ 3.54±0.30; **p <0.01; Figure 2C and 2D).

Both NR2A and NR2B, but not NR1, subunits were significantly increased in D2R-GSK-$3\beta^{-/-}$ mice (n=8, NR2A: D2R-GSK-$3\beta^{+/+}$ 1.00±0.15 vs. D2R-GSK-$3\beta^{-/-}$ 1.48±0.14, *p <0.05; NR2B: D2R-GSK-$3\beta^{+/+}$ 1.00±0.11 vs. D2R-GSK-$3\beta^{-/-}$ 1.41±0.15, *p <0.05; NR1: D2R-GSK-$3\beta^{+/+}$ 1.00±0.18 vs. D2R-GSK-$3\beta^{-/-}$ 1.01±0.43, p >0.05; Figure 3A). However, expression of AMPAR subunits GluR1 and GluR2 were unaffected in D2R-GSK-$3\beta^{-/-}$ mice (n=8, GluR1: D2R-GSK-$3\beta^{+/+}$ 1.00±0.09 vs. D2R-GSK-$3\beta^{-/-}$ 1.00±0.10, p >0.05; GluR2: D2R-GSK-$3\beta^{+/+}$ 1.00±0.13 vs. D2R-GSK-$3\beta^{-/-}$ 1.25±0.27, p >0.05; Figure 3A). To further examine whether AMPAR trafficking is affected, a membrane-impermeable protein cross-linker BS3 was used to separate surface and intracellular receptors. The surface proteins cross-linked with BS3 and formed large molecular congregate at ∼500 kD, which were easily separated from the small intracellular components (∼106 kD for GluR1 and ∼100 for GluR2) when detected via Western blot. Similar to total protein, both surface and intracellular AMPAR subunits were also not affected (n=4, surface GluR1: D2R-GSK-$3\beta^{+/+}$ 1.00±0.12 vs. D2R-GSK-$3\beta^{-/-}$ 1.10±0.11, p >0.05; Intracellular GluR1: D2R-GSK-$3\beta^{+/+}$ 1.00±0.12 vs. D2R-GSK-$3\beta^{-/-}$ 1.10±0.02, p >0.05; surface GluR2: D2R-GSK-$3\beta^{+/+}$ 1.00±0.13 vs. D2R-GSK-$3\beta^{-/-}$ 0.97±0.04, p >0.05; Intracellular GluR2: D2R-GSK-$3\beta^{+/+}$ 1.00±0.08 vs. D2R-GSK-$3\beta^{-/-}$ 1.24±0.39, p >0.05; Figure S5). Additionally, NR2B antagonist Ro 25-6981 (0.5 μM) significantly decreased amplitude but not decay time of the evoked NMDAR-mediated EPSCs in D2R-GSK-$3\beta^{-/-}$ mice vs. D2R-GSK-$3\beta^{+/+}$ mice. Additionally, the remaining amplitude of evoked NMDAR-mediated EPSCs after Ro 25-6981 treatment were significant higher in D2R-GSK-3β-/- mice compared with D2R-GSK-3β+/+ mice (n=10/group; amplitude: D2R-GSK-$3\beta^{+/+}$ -34.3±5.06% vs. D2R-GSK-$3\beta^{-/-}$ -54.2±6.69%, *p<0.05; decay times: D2R-GSK-$3\beta^{+/+}$ -29.5±6.56%

vs. D2R-GSK-3β$^{-/-}$ -49.7±9.91%, p>0.05; remaining amplitude: 1.00±0.22 vs. D2R-GSK-3β$^{-/-}$ 1.76±0.32, *p<0.05, Figure S6).

By western blotting, we found that HDAC2 protein was significantly decreased while HDAC4 protein was significantly increased in D2R-GSK-3β$^{-/-}$ mice (n=6 for each group, HDAC2 D2R-GSK-3β$^{+/+}$ 1.00±0.01 vs. D2R-GSK-3β$^{-/-}$ 0.46±0.07, *p <0.05; HDAC4 D2R-GSK-3β$^{+/+}$ 1.00±0.16 vs. D2R-GSK-3β$^{-/-}$ 1.63±0.12, *p <0.05; Figure 3B). As shown in Figure 3B, D2R-GSK-3β$^{-/-}$ mice had a dramatic increase in H3K27ac as well as H3K18ac (n=6 for each group, H3K27ac D2R-GSK-3β$^{+/+}$ 1.00±0.23 vs. D2R-GSK-3β$^{-/-}$ 1.81±0.24 *p <0.05; H3K18ac D2R-GSK-3β$^{+/+}$ 1.00±0.01 vs. D2R-GSK-3β$^{-/-}$ 1.24±0.06, *p <0.05). However, we did not detect a change in H3K9ac in D2R-GSK-3β$^{-/-}$ mice (n=6 for each group; D2R-GSK-3β$^{+/+}$ 1.00±0.24 vs. D2R-GSK-3β$^{-/-}$ 1.02±0.21, p >0.05). This data indicates that the increase in NMDAR expression in D2R-GSK-3β$^{-/-}$ mice may be attributed to the enrichment of site-specific acetylation on histone H3.

Grin2a and *Grin2b,* but not *Grin1,* at proximal promoter sites in D2R-GSK-3β$^{-/-}$ mice have a significant enrichment of H3K27ac in the mPFC compared with D2R-GSK-3β$^{+/+}$ (n=3 from 6 animals for each groups; H3K27ac *Grin2a*: D2R-GSK-3β$^{+/+}$ 0.22±0.04 vs. D2R-GSK-3β$^{-/-}$ 0.87±0.18 *p <0.05; H3K27ac *Grin2b*, D2R-GSK-3β$^{+/+}$ 1.22±0.07 vs. D2R-GSK-3β$^{-/-}$ 2.07±0.10, **p <0.01; H3K27ac *Grin1*, D2R-GSK-3β$^{+/+}$ 0.70±0.15 vs. D2R-GSK-3β$^{-/-}$ 0.10±0.25, p >0.05; Figure 3C left). In contrast, only *Grin2b,* but not *Grin2a* or *Grin1,* in D2R-GSK-3β$^{-/-}$ mice had a significant decrease in HDAC2 enrichment in the mPFC compared to their littermate controls (n=3 from 6 animals for each group; HDAC2 *Grin2a*; D2R-GSK-3β$^{+/+}$ 0.13±0.04 vs. D2R-GSK-3β$^{-/-}$ 0.07±0.02 p >0.05; HDAC2 *Grin2b*, D2R-GSK-3β$^{+/+}$ 1.24±0.13 vs. D2R-GSK-3β$^{-/-}$ 0.37±0.27, *p <0.05; HDAC2 *Grin1*, D2R-GSK-3β$^{+/+}$ 0.45±0.05 vs. D2R-GSK-3β$^{-/-}$ 0.40±0.26, p >0.05; Figure

3C right). Thus, HDAC2 enrichment is associated with increased H3K27ac enrichment at *Grin2b,* but not at *Grin2a*.

The number of trials to reach criterion for D2R mice showed a significant interaction effect by two-way ANOVA analysis (n=8 for each group, F=6.28, *p <0.05; Figure 4A). The simple effects test showed that the number of trials to reach criterion significantly increased after injection of MK-801 in D2R-GSK-3$\beta^{+/+}$ mice compared with injection of saline in either D2R-GSK-3$\beta^{+/+}$ mice or D2R-GSK-3$\beta^{-/-}$ mice (D2R-GSK-3$\beta^{+/+}$ saline 98.1±20.6 vs. D2R-GSK-3$\beta^{+/+}$ MK-801 170.5±18.62; D2R-GSK-3$\beta^{-/-}$ saline 113.4±7.11 vs. D2R-GSK-3$\beta^{+/+}$ MK-801 170.5±18.6, *p <0.05 for both; Figure 4A), demonstrating the expected MK-801-induced cognitive deficit in wild-type animals. Interestingly, injection of MK-801 in D2R-GSK-3$\beta^{-/-}$ mice resulted in fewer number of trials to criterion compared with the performance of D2R-GSK-3$\beta^{+/+}$ mice treated with MK-801 (D2R-GSK-3$\beta^{+/+}$ MK-801 170.5±18.6 vs. D2R-GSK-3$\beta^{-/-}$ MK-801 120.4±16.2; *p <0.05; Figure 4A), suggesting that D2R-GSK-3$\beta^{-/-}$ exhibited a decreased sensitivity to MK801, prohibiting the expected deficits in cognitive function caused by the NMDAR antagonist. We also analyzed the three types of errors commonly observed in this task by two-way ANOVA. However, we did not detect any significant changes in three different errors (perseverative errors: interaction F=1.78, p >0.05, treatment F=0.46, p >0.05, genotype F=0.02, p >0.05; regressive errors: interaction F=2.66, p >0.05, treatment F=0.12, p >0.05, genotype F=2.89, p >0.05; never reinforced errors: interaction F=0.02, p >0.05, treatment F=0.14, p >0.05, genotype F=0.12, p >0.05, Figure 4B).

For D1 mice, two-way ANOVA revealed that the main effect of treatment was significant (n=8 for each group, F=9.82, **p <0.01; Figure S7A) but the main effect of genotype was not significant (F=0.05, p >0.05; Figure S7A). The post hoc t-test indicated that the number of trials to reach criterion significantly increased in both D1R-GSK-3$\beta^{+/+}$ and D1R-GSK-3$\beta^{-/-}$ mice after MK-801

treatment compared with the effect of saline on both groups (D1R-GSK-3β$^{+/+}$ saline 95.8±11.8 vs. D1R-GSK-3β$^{+/+}$ MK-801 164.2±16.3, D1R-GSK-3β$^{-/-}$ saline 112.3±12.1 vs. D1R-GSK-3β$^{-/-}$ MK-801 170.2±19.4, *p <0.05 for both; Figure S2A). Further, there is no significant difference between D1R-GSK-3β$^{+/+}$ MK-801 vs. D1R-GSK-3β$^{-/-}$ MK-801 (p >0.05). We also analyzed the three types of errors commonly observed in this task by two-way ANOVA. We did not detect any significant differences in three different errors (perseverative errors: interaction F=0.75, p >0.05, treatment F=0.53, p >0.05, genotype F=0.26, p >0.05; regressive errors: interaction F=0.71, p >0.05, treatment F=0.23, p >0.05, genotype F=0.77, p >0.05; never reinforced errors: interaction F=3.08, p >0.05, treatment F=2.94 p >0.05, genotype F=1.17, p >0.05, Figure S7B).

As shown in Figure 5A, pGSK-3β-Ser9 was significantly decreased while pGSK-3β-Tyr216 was increased in mutant hDISC1 mice (n=6 for each group, pGSK-3β-Ser9: control mice 1.00±0.15 vs. mutant hDISC1 mice 0.28±0.55; pGSK-3β-Tyr216: control mice 1.00±0.17 vs. mutant hDISC1 mice 1.88±0.17; **p <0.01 for both; Figure 5A), whereas the total protein level of GSK-3β was unaltered (n=6 for each group, control mice 1.00±0.44 vs. mutant hDISC1 mice 0.79±0.32, p >0.05; Figure 5A). Since GSK-3β activity is down-regulated by pGSK-3β-Ser9 and up-regulated by pGSK-3β-Tyr216, these results strongly suggest that GSK-3β activity is enhanced in mutant hDISC1 mice(12). Further, we found that NR2B subunit protein levels were significantly decreased, but neither NR2A nor NR1 subunit expression levels changed in mutant hDISC1 mice (n=6 for each group, NR2B: control mice 1.00±0.09 vs. mutant hDISC1 mice 0.62±0.09, *p <0.05; NR2A: control mice 1.00±0.33 vs. mutant hDISC1 mice 0.82±0.19, p >0.05; NR1: control mice 1.00±0.09 vs. mutant hDISC1 mice 1.04±0.16, p >0.05; Figure 5A).

The amplitude of NMDAR-mEPSCs was significantly decreased in mutant hDISC1 mice without a change in frequency (n=18 for each group, amplitude: control mice 16.3±4.42 vs. mutant

hDISC1 mice 11.5±1.51, p <0.01; frequency: control mice 0.51±0.05 vs. mutant hDISC1 mice 0.43±0.04, p >0.05; Figure 5B). However, there was no significant difference in NMDAR-sEPSCs between mutant hDISC1mice and their littermate controls (n=18 for each group, sEPSCs amplitude: control mice 14.6±0.91 vs. mutant hDISC1 mice 15.5±0.98, p >0.05; sEPSCs frequency: control mice 0.72±1.00 vs. mutant hDISC1 mice 0.79±0.07, p >0.05; Figure 5B). There was also no difference in either AMPAR-sEPSCs or AMPAR-mEPSCs between mutant hDISC1 mice and their littermate controls (data not shown, n=12 for each group, sEPSCs amplitude: control mice 11.5±0.73 vs. mutant hDISC1 mice 11.8±0.86, p >0.05; sEPSCs frequency: control mice 1.07±0.11 vs. mutant hDISC1 mice 0.86±0.12, p >0.05; mEPSCs amplitude: control mice 11.0±1.24 vs. mutant hDISC1 mice 12.9±2.71, p >0.05; mEPSCs frequency: control mice 0.60±0.04 vs. mutant hDISC1 mice 0.56±0.03, p >0.05). Together, these results suggest that mutant hDISC1 specifically and negatively regulates NMDAR function via increased activity of GSK-3β.

As illustrated in Figure 5C, in vivo SB216763 injection rescued the reduced NMDAR-mEPSC amplitude in mutant hDISC1 mice (n=12 for each group, sEPSCs amplitude: control mice 16.1±1.67 vs. mutant hDISC1 mice 14.6±1.60, p >0.05; sEPSCs frequency: control mice 0.84±0.17 vs. mutant hDISC1 mice 0.52±0.12, p >0.05; mEPSCs amplitude: control mice 11.9±0.60 vs. mutant hDISC1 mice 15.00±0.83, **p <0.01; mEPSCs frequency: control mice 0.69±0.13 vs. mutant hDISC1 0.53±0.14, p >0.05). To investigate whether mutant hDISC1-induced down-regulation of NMDAR function is due to increased interaction of the D2R-DISC1 complex, we disrupted D2R-DISC1 interaction with TAT-D2pep [K211-T225] (KIYIVLRRRRKRVNT; 10 μM), a peptide that effectively interferes with the interaction between D2Rs and DISC1 (13). Mutant hDISC1 mice received once daily I.P. injections of either TAT-

D2pep [K211-T225] (10 μM) or scrambled control peptide (D2pep-sc; VLRKTRIRRYKIRNV; 10 μM) beginning at P25 and continuing for 5 consecutive days. Similar to treatment with GSK-3β inhibitor, TAT-D2pep [K211-T225] reversed the decreased amplitude of NMDAR-mEPSCs in mutant hDISC1 mice compared with the scrambled control peptide (D2pep-sc) (n=10 for each group, sEPSCs amplitude: TAT-D2pep-sc 14.7±0.51 vs. TAT-D2pep 13.6±1.18, $p > 0.05$; mEPSCs amplitude: TAT-D2pep-sc 11.7±0.69 vs. TAT-D2pep 15.0±0.99, $p < 0.01$; Figure 5D right). In addition to the change in EPSC amplitude, TAT-D2pep [K211-T225] caused a significant decrease in NMDAR-sEPSC frequency but no change in NMDAR-mEPSC frequency (n=10 for each group, sEPSCs frequency: TAT-D2pep-sc 1.00±0.07 vs. TAT-D2pep 0.64±0.10, $^{*}p < 0.05$; mEPSCs frequency: TAT-D2pep-sc 0.33±0.10 vs. TAT-D2pep 0.38±0.09, $p > 0.05$; Figure 5D left).

Supplemental Discussion

First, DA receptors in the PFC are known to exert powerful effects on cognition by modulating synaptic transmission, especially NMDAR function. Specifically, D2Rs modulate NMDARs via GSK-3β signaling (2, 14). Interestingly, we found that global conditional deletion of GSK-3β significantly increased NMDAR-EPSCs in the mPFC of D2R-, but not D1R-, GSK-3$\beta^{-/-}$ mice. In addition, global ablation of GSK-3β in D2R+ neurons disrupts the balance of D1R- vs D2R-dependent modulation of NMDAR-EPSCs in the mPFC. In previous studies, we and others have reported that GSK-3β is critical for the dose-dependent modulation of NMDAR function in a D2R-dependent manner (2, 15-17), which is derived from the change of NMDAR expression and trafficking. Here, we replicated this finding and further revealed an enhanced sensitivity of NMDAR-mediated function and a shifted response to DA. The overall effect of DA modulation is

to promote NMDAR function; therefore, global deletion of GSK-3β in D2R-expressing neurons led to an enhanced DA modulation of NMDAR function in the mPFC, which is caused by the loss of GSK-3β-D2R signaling-mediated change of NMDAR expression and/or trafficking as our previous study reported (2).

Previous studies have reported that CRISPR/Cas9 or Cre-mediated knockout, or inhibition, of GSK3β in adult mPFC and other cortical and hippocampal regions decreases AMPA-sEPSC (18-21). Surprisingly, we didn't detect any significant change of AMPAR-EPSCs in the mPFC of D2R-GSK-3β$^{-/-}$ mice. The reason for this discrepancy is likely that we knocked out GSK3β during neurodevelopment in D2R-Cre mice, while other studies reporting AMPA-mediated effects by knockout of GSK-3β in adult mice (18, 19), suggesting a possible system-wide neurodevelopmental effect of GSK-3β in the current study. Furthermore, our results also indicate a novel cell-type specific role of GSK-3β in regulating NMDAR and AMPAR function, i.e., GSK-3β may specifically modulate NMDAR in D2R+ but AMPAR in non-D2R+ neurons in the mPFC (Li et al, unpublished observations). Furthermore, this finding also supports our previous studies about the role of GSK-3β in normal mPFC, in which D2R-mediated regulation of NMDAR function is required the normal activities of GSK-3β (2).

NMDARs play a key role in the neurochemical and neurophysiological basis of learning and memory, which is often referred to as long-term plasticity (22). GSK-3β is also a critical player in both LTP and LTD (23, 24). In addition, studies have shown that growth or enlargement of spines is associated with induction of LTP, whereas LTD-inducing stimulation causes shrinkage or retraction of spines (25-28). Consistent with the long-term plasticity changes detected in D2R-GSK-3β$^{-/-}$ mice, we found that spine number in apical dendrites of PFC layer V, but not layer II/III, pyramidal neurons, is significantly increased in D2R-GSK-3β$^{-/-}$ mice. It is not surprising that

pyramidal neurons in layer II/III and layer V did not exhibit a similar change in spine number by loss of GSK-3β as pyramidal neurons located in different cortical layers exhibit variable connectivity, dendritic morphology, and functional properties (29, 30). However, it has been reported that deletion of GSK-3β in adult mPFC did not affect spine density (19), while knockout of GSK-3β in adult hippocampus decreased the spine density (18). These inconsistent effects on the spine quantity induced by deletion of GSK-3β at different ages or brain regions suggest a potential developmental and cell-type specific effect of GSK-3β reported in our study. Increases in spine number or turnover correlate with the ability to learn new tasks (31). In post-mortem tissue from SZ subjects, dendritic spines are reduced in prefrontal cortical pyramidal neurons (32, 33). This may be associated with cognitive dysfunction in SZ due to the reduced anatomic basis for NMDARs, or secondary loss of NMDARs (34). Therefore, an increase in spine density in mPFC layer V pyramidal neurons as we report here may contribute to the improvement of cognitive function in D2R-GSK-3$\beta^{-/-}$ mice.

We found that both NR2A and NR2B NMDAR subunits were increased in the mPFC tissue of D2R-GSK-3$\beta^{-/-}$ mice, whereas no corresponding change in the obligatory NR1 subunit was detected in D2R-GSK-3$\beta^{-/-}$ mice. This is probably attributable to the compensatory decrease of NR3A (Li et al, unpublished observations). The NR3A subunit is a known negative regulator of NMDAR current, related to the induction of LTP (35-38). Although the exact contribution of NR2A and NR2B to synaptic plasticity has been debated, it appears that NR2A/NR2B ratio is a critical determinant for the change of LTP and LTD (39-42). Therefore, the increase of NR2A and NR2B, accompanied by a concomitant decrease of NR3A, induced by deletion GSK-3β in D2R+ neurons, could all possibly contribute to the imbalance of LTP and/or LTD observed (Figure 2). Also, in the BS3 crosslink assay, we did not detect any significant changes of either total or surface

protein levels of AMPAR at the basal condition in D2RGSK3β-/- mice. However, previous studies indicated that GSK3β is required for regulated AMPAR endocytosis during LTD induction (43). Therefore, our result cannot exclude the potential of knockout of GSK3β in D2+ neurons affecting AMPAR trafficking during LTD induction. Based on this report, GSK3β KO would disrupt regulated AMPAR endocytosis during LTD, which in turn, would eliminate LTD induction. Indeed, consistently, LTD was terminated in D2RGSK3β-/- KO mice. Additionally, as LTP inhibits LTD induction via the GSK3β-PI3K-Akt pathway (44), we cannot rule out the possibility that the disrupted LTD is induced by the increased LTP in D2RGSK3β-/- mice.

A question raised here is the mechanism underlying the increase in NR2 expression. Epigenetic processes are increasingly implicated in developmental changes of NMDARs (45, 46), as well as the pathophysiology of SZ and other psychiatric disorders (47, 48). During development, epigenetic mechanisms can alter gene expression profiles due to either environmental or genetic inputs, therefore modifying brain development and memory formation (6, 49, 50). To this end, increasing evidence shows that NMDAR subunit expression can be altered through various epigenetic changes. For example, distal regulatory *Grin2b* sequences controlled by H3K4me and H3K9me are highly associated with the maintenance of working memory (51). Our recent study also reported that a global increase of the repressive mark H3K27me3 is highly enriched in the *Grin2b* proximal promoter region, contributing to down-regulation of NMDAR expression and concomitantly synaptic function in the developing PFC of prenatally methylazoxymethanol acetate (MAM)-exposed rats (52). Further, GSK-3β can phosphorylate several histone deacetylases (HDACs) resulting in altered HDACs activity (53-56). A recent study also demonstrated that inhibition of HDACs increases the expression of NR2B in the hippocampus by enhancing histone acetylation (57). Thus, we asked whether deletion of GSK-3β leads to a decrease in HDAC2

activity and increased histone acetylation, which may contribute to the increase in NR2B and/or NR2A protein expression observed in D2R-GSK-3β$^{-/-}$ mice. We tested this possibility by measuring HDAC2 and HDAC4 total protein levels, as both are closely related to synaptic transmission and plasticity (58, 59). We found a significant decrease in HDAC2 and a marked increase in HDAC4 protein levels in the mPFC of D2R-GSK-3β$^{-/-}$ mice. It has been reported that GSK-3β can trigger HDAC4 degradation by phosphorylating the sequence that controls HDAC4 stability (55). Consequently, knockout of GSK-3β can induce an increase of HDAC4 expression by decreasing its degradation. Notably, HDAC4 is a positive regulator of synaptic plasticity (59) while HDAC2 negatively regulates dendritic spine density (58). Thus, the increase in HDAC4 levels and decrease in HDAC2 levels in layer V pyramidal neurons of D2R-GSK-3β$^{-/-}$ mPFC support the enhanced synaptic plasticity and increased spine density we observed in this study. Consistent with a decrease of HDAC2 levels, we also found a significant increase of overall histone acetylation at H3K27 and H3K18 residues of the histone H3 tail. ChIP assays further confirmed that activation mark H3K27ac was highly enriched at the promoter of both *Grin2a* and *Grin2b*. However, a significant decrease in HDAC2 enrichment was only detected at *Grin2b,* but not *Grin2a,* although there is a trending decrease. It is possible that a low level of HDAC2 enrichment already exists at the *Grin2a* promoter in the control mice, making it difficult to detect significant changes in HDAC2 levels in D2R-GSK-3β$^{-/-}$ mice. Additionally, a remarkable 50% decrease of total HDAC2 levels failed to alter *Grin1* and *Grin2a* genes in the D2R-GSK-3β$^{-/-}$ mice, hence we cannot rule out that the decrease of HDAC2 protein levels also contributed to the modulation of another gene expression beyond of *Grin2b*. The pattern of HDAC2 enrichment in either control mice or mutant mice across promoters is *Grin2b* > *Grin1* > *Grin2a*, suggesting that *Grin2b* expression is more tightly regulated than other NMDAR subunit proteins by HDAC2.

We and other's studies indicated the important role of cortical GSK-3β in maintaining different cognitive function such as working memory and reward processing (60-62). In addition, the PFC mediates highly complex cognitive functions that require the flexible use of information from multiple cortical areas, which can be well-described by tasks such as attention set-shifting (63, 64), which is highly related to both NMDARs and the DA system in the mPFC. Specifically, lesions to the mPFC cause a selective impairment in extradimensional shifts but have no effect on reversal learning (65). MK-801 and other antagonists blocking cortical NMDARs impair set-shifting, although the learning and maintenance of a new strategy remain unaffected (66-69). Here, our study shows that D2R-GSK-3β$^{-/-}$ mice, but not D1R-GSK-3β$^{-/-}$ mice, are resistant to MK-801-induced impairment in set-shifting, suggesting that NMDAR-dependent cognitive flexibility was not affected by MK-801 after deletion of GSK-3β in D2R+ neurons. Consistently, we and others reported that global inhibition of GSK-3β by GSK-3β inhibitor during development can rescue the spatial working memory deficit (60, 70). It is plausible that this rescue effect may also be mediated by GSK-3β in D2R-expressing neurons. Additionally, our previous study reported that D2R-GSK-3β$^{-/-}$ mice showed enhanced cognitive performance in a Y-maze-based test that is used to evaluate working memory function. In the present study, however, D2R-GSK-3β$^{-/-}$ mice treated with saline showed no better performance in the set-shifting task than their littermate controls, probably due to the distinct anatomical pathways engaged during working memory and set-shifting processes (67, 71, 72). Furthermore, LTD induced in the hippocampus is reported to facilitate behavioral flexibility in the Water Maze task (73-75). However, we observed improved cognitive flexibility with the Cross Maze task, which relies more heavily on the mPFC (76) in D2RGSK3β-/- mice. We believe the increased behavioral flexibility in D2RGSK3β-/- mice is likely due to an increased LTP in prefrontal neurons, although this assumption remains to be tested in the future study.

Finally, a recent study reported that DISC1 protein can form a complex with D2Rs to modulate GSK-3β signaling (13). Specifically, GSK-3β activity is enhanced by an increased interaction between D2Rs and DISC1 in Disc1-L100P mutant mice and SZ patients (13). Consistent with this report, we found an enhanced GSK-3β activity that is accompanied by a decreased NMDAR function in mice expressing a mutant (truncated) human DISC1 gene. Importantly, the reduced NMDAR-mediated currents were effectively reversed, not only by inhibiting GSK-3β activity with selective inhibitor but also by interrupting D2R-DISC1 interactions with TAT-D2 peptide during the adolescent period. These data provide strong evidence that GSK-3β modulation of NMDAR function is closely associated with D2R-DISC1 interaction. We also noticed that disrupting D2R-DISC1 interaction by administering TAT-D2pep [K211-T225] caused a significant decrease in the frequency of NMDAR-sEPSCs, but not the frequency of NMDAR-mEPSCs, in mutant hDISC1 mice compared with controls. This suggests a possible pre-synaptic effect of DISC1 on neurotransmitter release that is influenced by TAT-D2pep [K211-T225] (77, 78). Moreover, although a decrease of NMDAR expression levels was detected in mutant hDISC1 mice, only the NR2B (but not NR2A) subunit was significantly altered, indicating that DISC1-mediated D2R-GSK-3β signaling mainly affects NR2B and other mechanisms might control D2R-GSK-3β regulation of NR2A.

Supplemental Figures

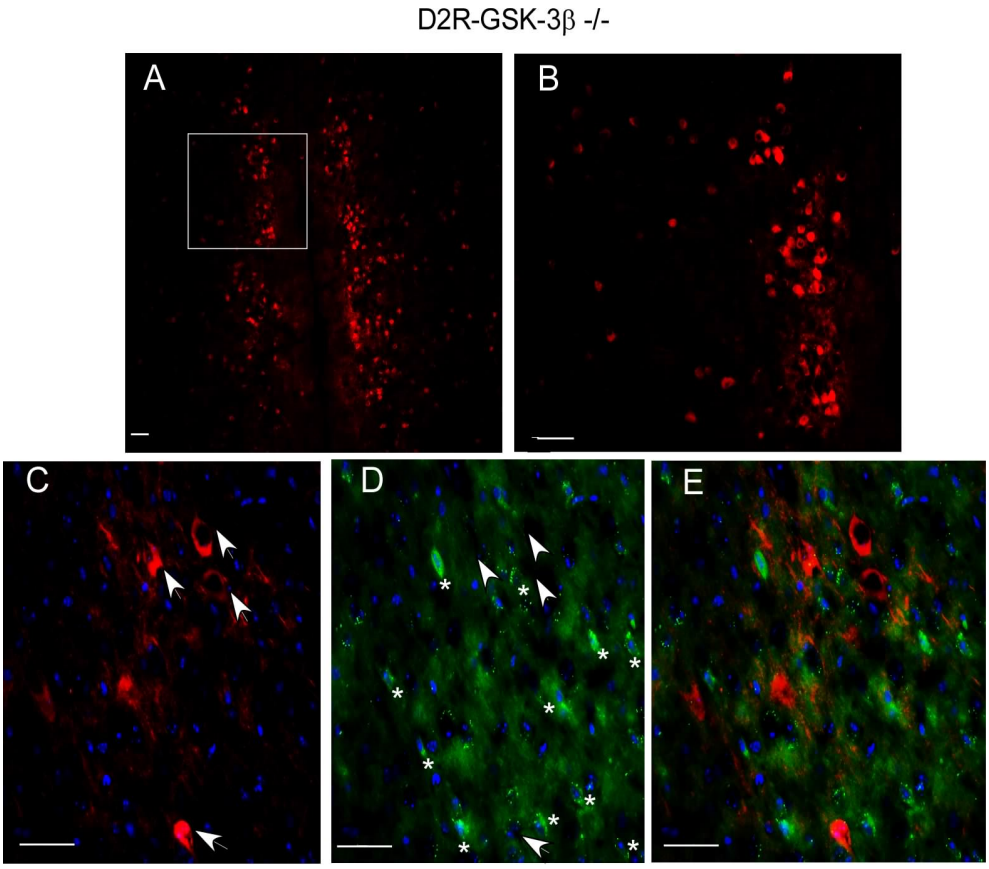

Figure S1. Cre expression and GSK-3β deletion in the PFC region of D2R-GSK-3β-/- mice. A and B, neurons expression in the PFC of D2R-GSK-3β-/- mice contains Cre-dependent Tomato reporter. C, typical Cre-Tomato-labeled D2R-expressing neurons (arrowheads). D, typical GFP-labeled GSK-3β-positive neurons (stars). E, lack of GSK-3β in Tomato-labeled D1R- or D2R-expressing neurons. Scale bar: 50 μm.

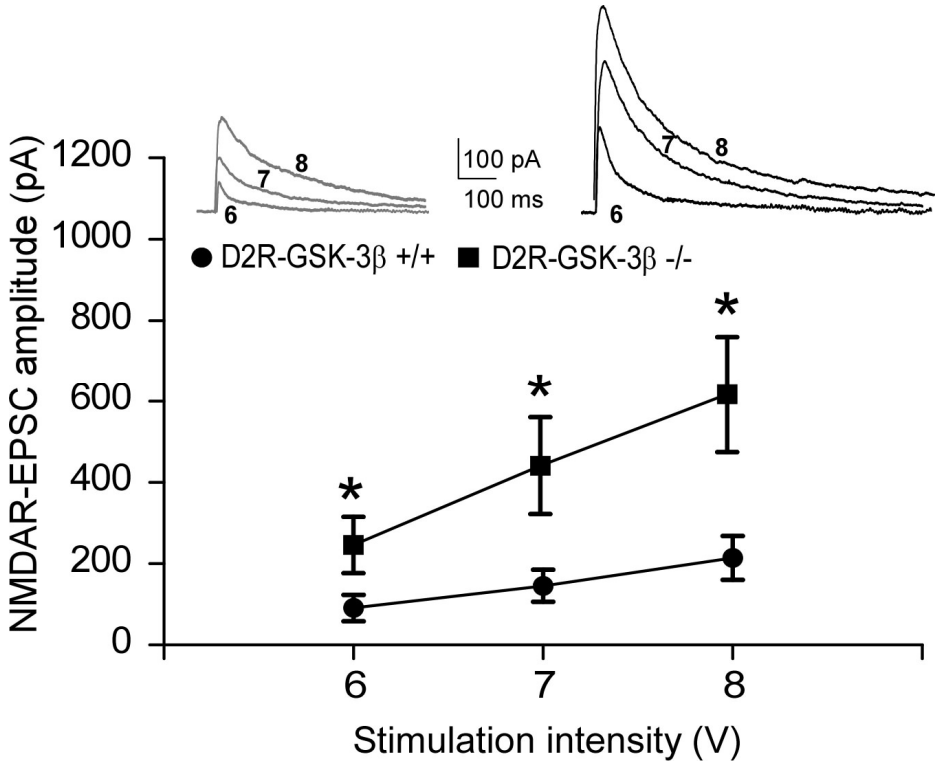

Figure S2. The input-output curves of evoked NMDAR-EPSCs in D2R-GSK-3β$^{-/-}$ and D2R-GSK-3β$^{+/+}$ mice. Represented traces of evoked NMDAR-eEPSCs in response to a series of stimulation intensities were recorded from layer V pyramidal neurons in the mPFC (upper panel). D2R-GSK-3β$^{-/-}$ mice showed a significant increase of NMDAR-eEPSC amplitude in response to all three intensities compared with that of D2R-GSK-3β$^{+/+}$ mice (lower panel, n=11/group, two-way repeated measures ANOVA followed by Post-hoc tests. $F = 6.05$, *$p < 0.05$, stimulation intensity: $F = 18.5$, ***$p < 0.01$; Post-hoc tests: *$p < 0.05$ for all intensities).

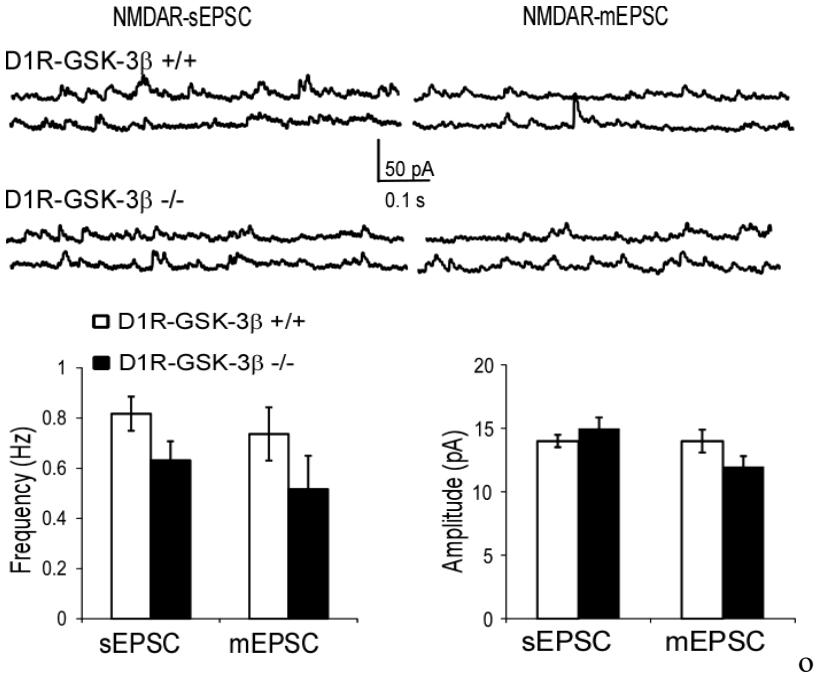

Figure S3. To confirm cell-type specificity of the increase in NMDAR-EPSCs in D2R-GSK-3β$^{-/-}$ mice, we crossed GSK-3β$^{flox/flox}$ mice with Drd1-Cre mice to generate D1R-GSK-3β$^{-/-}$ mice. Deletion of GSK-3β in D1R+ (D1R-GSK-3β$^{-/-}$) did not affect NMDAR-mediated currents in layer V pyramidal neurons of mouse mPFC. Sample traces of NMDAR-sEPSCs and NMDAR-mEPSCs were recorded from layer V pyramidal neurons in the PFC (upper panel). Summary histograms in the lower panel demonstrate no difference of NMDAR-EPSCs between D1R-GSK-3β$^{+/+}$ and D1R-GSK-3β$^{-/-}$ (n=16/group, $p > 0.05$ for all).

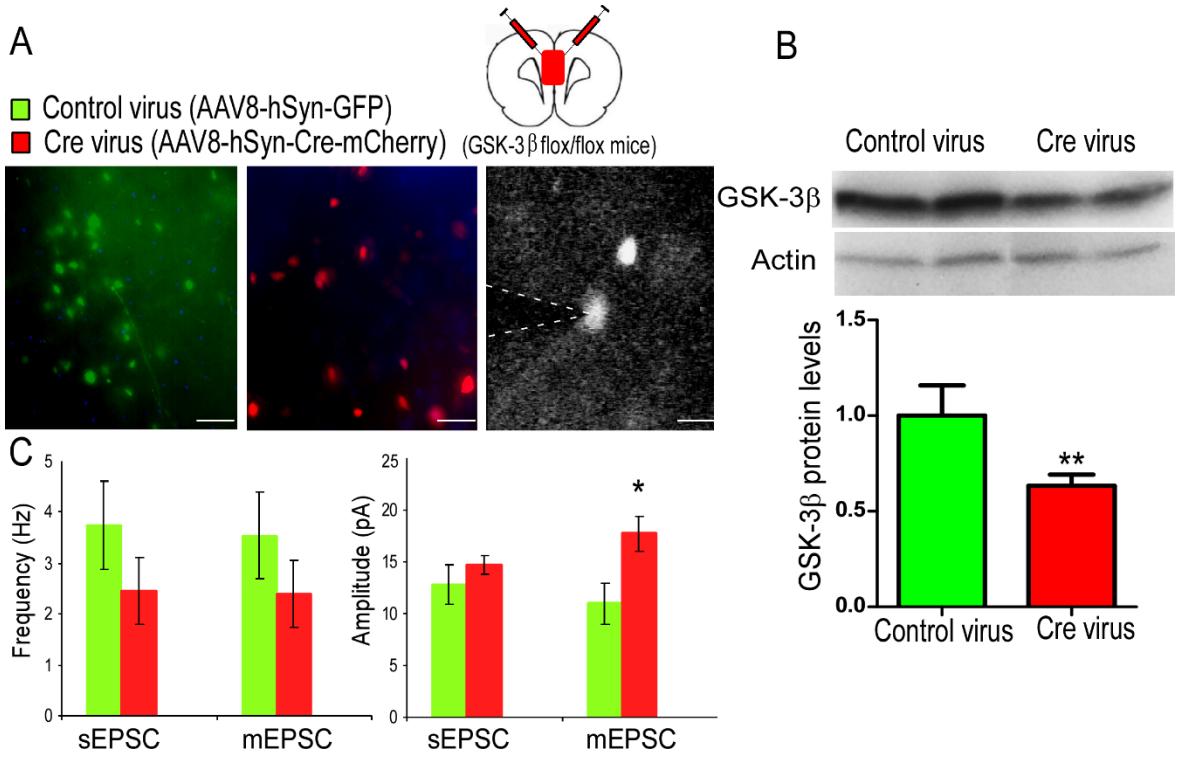

Figure S4. Local ablation of GSK-3β in the PFC similarly potentiates NMDAR function. A, control virus (AAV8-hSyn-GFP) and Cre virus (AAV8-hSyn-Cre-mCherry) expressed in the PFC after five weeks of injection. Scale bar: 50 μm. B, GSK-3β total protein levels in the mPFC were significantly decreased in Cre virus group vs control virus group after three weeks of injection (*p<0.01; n=2). C, injection of Cre virus into the mPFC at P25 of GSK-3β$^{flox/flox}$ mice increased the amplitude of NMDAR–mEPSC compared with that of the control virus injection group, although the amplitude of sEPSCs and frequency of both sEPSCs and mEPSCs were unchanged (n=6/group, Cre virus group vs. control virus group, *p <0.05 for amplitude of NMDAR–mEPSC; p>0.05 for amplitude of sEPSCs, frequency of both sEPSCs and mEPSCs).

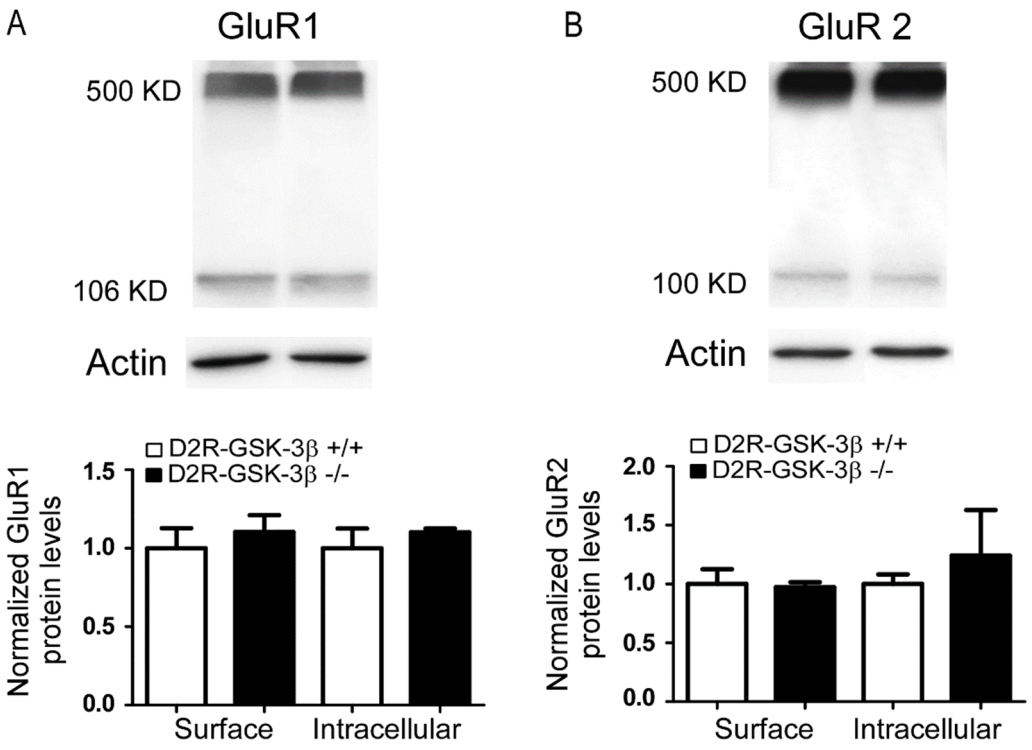

Figure S5. Deletion of GSK-3β in D2R+ (D1R-GSK-3$\beta^{-/-}$) did not affect AMPAR trafficking. A, representative Western blots showed that either surface or intracellular GluR1 protein levels from the mPFC of D2R-GSK-3β+/+ and D2R-GSK-3β-/- mice after treatment with BS3. Summary histograms showed that both surface and intracellular GluR1 protein levels were unaffected in D2R-GSK-3β-/- mice compared with D2R-GSK-3$\beta^{+/+}$ mice (n=4/group, p >0.05 for both). B, representative Western blots showed that either surface or intracellular GluR2 protein levels from the mPFC of D2R-GSK-3β+/+ and D2R-GSK-3β-/- mice after treatment with BS3. Summary histograms showed that both surface and intracellular GluR1 protein levels were unchanged in D2R-GSK-3β-/- mice compared with D2R-GSK-3$\beta^{+/+}$ mice (n=4/group, p >0.05 for both).

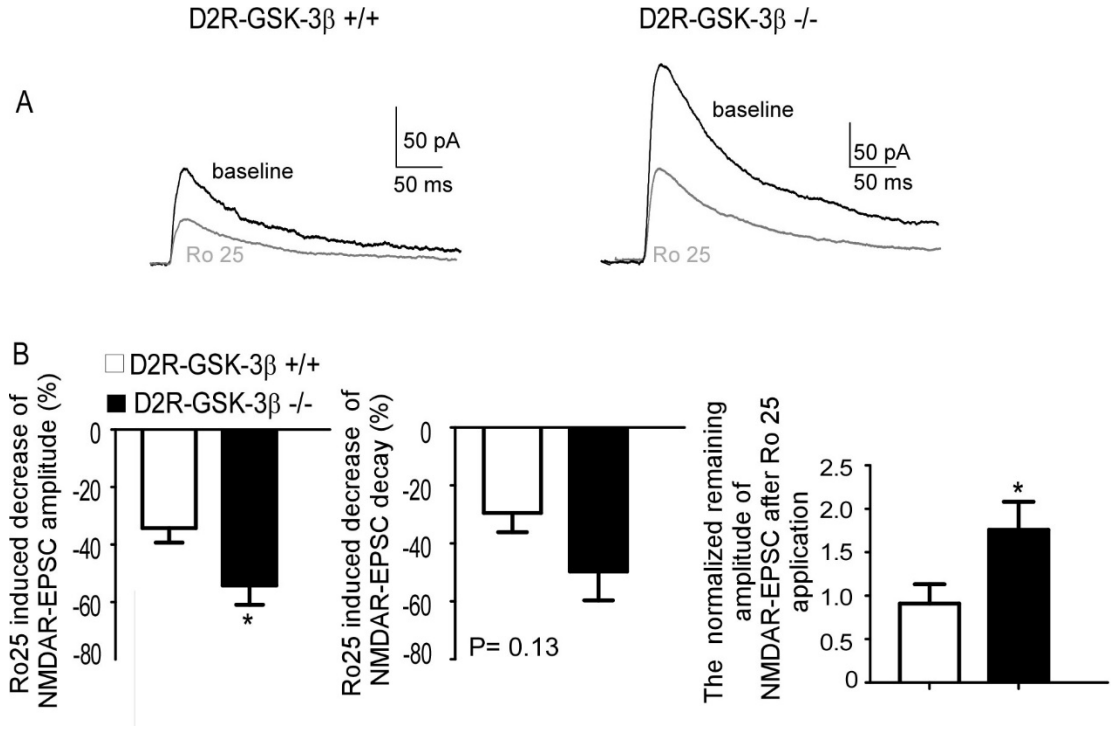

Figure S6. NR2B antagonist Ro 25-6981 differentially affects evoked NMDAR-EPSCs in D2R-GSK-3$\beta^{-/-}$ and D2R-GSK-3$\beta^{+/+}$ mice. A, representative evoked NMDAR-EPSC traces at baseline and after bath application of Ro 25-6981 (Ro 25, 0.5 μM). B, Summary histograms showed that the amplitude but not decay time of NMDAR-EPSCs was significantly reduced in D2R-GSK-3β-/- mice compared with D2R-GSK-3β+/+ mice after Ro 25 application (n=10/group, *p<0.05 for amplitude and p>0.05 for decay time; stimulation intensity both at 7V). The remaining amplitude of NMDAR-EPSCs was still significantly higher in D2R-GSK-3β-/- mice compared with D2R-GSK-3β+/+ mice after Ro 25 application (n=10/group, *p<0.05; stimulation intensity both at 7V).

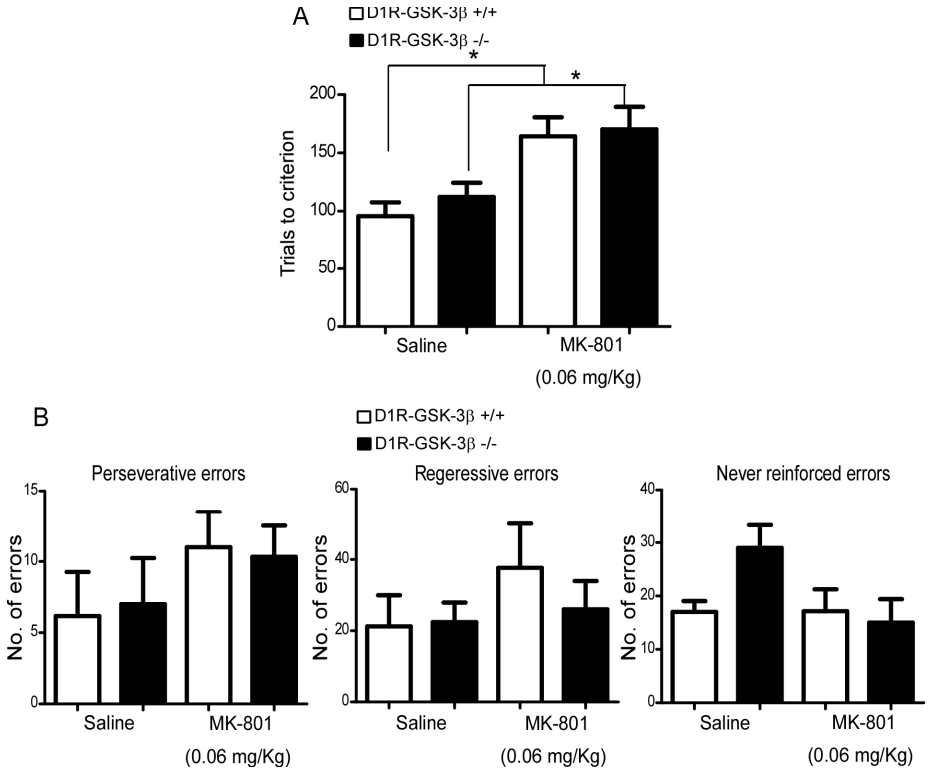

Figure S7. D1R-GSK-3β$^{-/-}$ mice cannot resist MK-801-induced working memory deficits. A, two-way ANOVA revealed that the main effect of treatment was significant (n=8, F=9.82, **p < 0.01) but the main effect of genotype was non-significant (F=0.05, p > 0.05). Post-hoc t-tests indicated that the number of trials to criterion was significantly increased in both D1R-GSK-3β$^{+/+}$ mice and D1R-GSK-3β$^{-/-}$ after injection of MK-801 compared with injection of saline in both genotypes (*p < 0.05 both). Nonetheless, there were no significant differences in trials to criterion between D1R-GSK-3β$^{+/+}$ MK-801 and D1R-GSK-3β$^{-/-}$ MK-801 (p > 0.05). B, No significant differences were detected in three types of error among D1R-GSK-3β$^{+/+}$ saline, D1R-GSK-3β$^{+/+}$ MK-801, D1R-GSK-3β$^{-/-}$ saline and D1R-GSK-3β$^{-/-}$ MK-801 (perseverative errors: interaction F=0.75, p > 0.05, treatment F=0.53, p > 0.05, genotype F=0.26, p > 0.05; regressive errors: interaction F=0.71, p >0.05, treatment F=0.23, p >0.05, genotype F=0.77, p >0.05; never reinforced errors: interaction F=3.08, p >0.05, treatment F=2.94, p >0.05, genotypes F=1.17, p >0.05).

Figure S8. The expression of mutant hDISC1 in both control and mutant hDISC1 mice. Myc peptide is used as a marker that was fused into mutant N-terminals of hDISC1 protein. Mutant hDISC1 proteins were visualized in the mPFC of mutant hDISC1 mice but not in control mice.

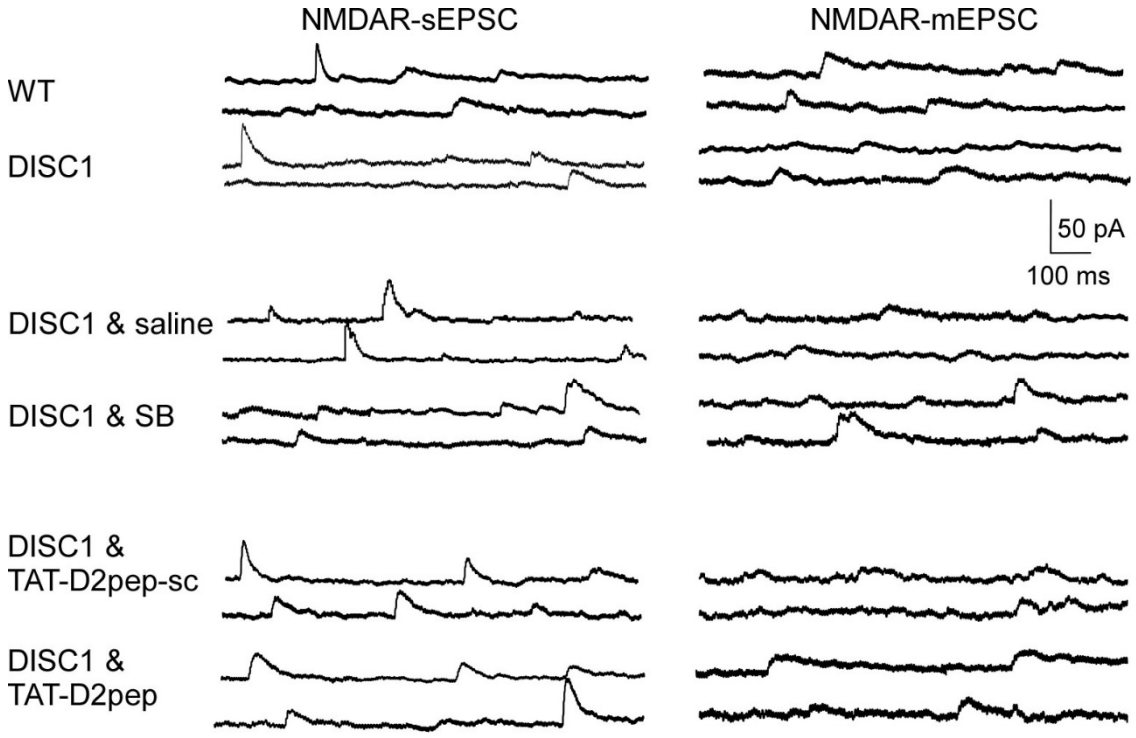

Figure S9. Sample traces of NMDAR-sEPSCs and NMDAR-mEPSCs recorded from layer V pyramidal neurons in the mPFC of wild type control mice, and mutant hDISC1 with different drug treatments.

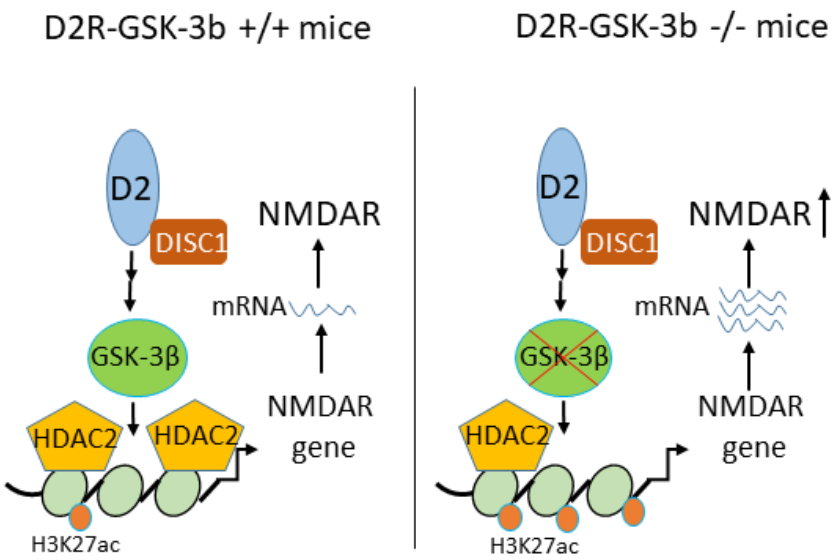

Figure S10. A schematic graph showing GSK-3β regulation of NMDAR expression in D2R-expressing neurons. In D2R-GSK-3β$^{+/+}$ mice, D2Rs and DISC1 form a complex that activates GSK-3β signaling, modulating NMDAR expression via HDAC2 and H3K27ac epigenetic control at the proximal promoter region of either *Grin2A* or *Grin2B*. In D2R-GSK-3β$^{-/-}$ mice, deletion of GSK-3β in D2R-expressing neurons disrupts GSK-3β signaling mediated by D2R/DISC1 interactions. As a result, a decrease in HDAC2 levels and/or an increase in H3K27ac levels will promote NMDAR gene expression, which consequently enhances NMDAR function in the excitatory synapses of mPFC pyramidal neurons.

Supplemental References

1. Urs NM, Snyder JC, Jacobsen JPR, Peterson SM, Caron MG (2012): Deletion of GSK3beta in D2R-expressing neurons reveals distinct roles for Î²-arrestin signaling in antipsychotic and lithium action. *Proceedings of the National Academy of Sciences*. 109:20732-20737.
2. Li YC, Xi D, Roman J, Huang YQ, Gao WJ (2009): Activation of glycogen synthase kinase-3 beta is required for hyperdopamine and D2 receptor-mediated inhibition of synaptic NMDA receptor function in the rat prefrontal cortex. *The Journal of neuroscience : the official journal of the Society for Neuroscience*. 29:15551-15563.
3. Arango-Lievano M, Schwarz JT, Vernov M, Wilkinson MB, Bradbury K, Feliz A, et al. (2014): Cell-type specific expression of p11 controls cocaine reward. *Biological psychiatry*. 76:794-801.
4. Kaspar BK, Vissel B, Bengoechea T, Crone S, Randolph-Moore L, Muller R, et al. (2002): Adeno-associated virus effectively mediates conditional gene modification in the brain. *Proceedings of the National Academy of Sciences of the United States of America*. 99:2320-2325.
5. Wang MJ, Li YC, Snyder MA, Wang H, Li F, Gao WJ (2013): Group II metabotropic glutamate receptor agonist LY379268 regulates AMPA receptor trafficking in prefrontal cortical neurons. *PloS one*. 8:e61787.
6. Rodenas-Ruano A, Chavez AE, Cossio MJ, Castillo PE, Zukin RS (2012): REST-dependent epigenetic remodeling promotes the developmental switch in synaptic NMDA receptors. *Nature neuroscience*. 15:1382-1390.
7. Cubelos B, Sebastian-Serrano A, Beccari L, Calcagnotto ME, Cisneros E, Kim S, et al. (2010): Cux1 and Cux2 regulate dendritic branching, spine morphology, and synapses of the upper layer neurons of the cortex. *Neuron*. 66:523-535.
8. Xing B, Li YC, Gao WJ (2016): GSK3beta Hyperactivity during an Early Critical Period Impairs Prefrontal Synaptic Plasticity and Induces Lasting Deficits in Spine Morphology and Working Memory. 41:3003-3015.
9. Li ML, Yang SS, Xing B, Ferguson BR, Gulchina Y, Li YC, et al. (2015): LY395756, an mGluR2 agonist and mGluR3 antagonist, enhances NMDA receptor expression and function in the normal adult rat prefrontal cortex, but fails to improve working memory and reverse MK801-induced working memory impairment. *Exp Neurol*. 273:190-201.
10. LaCrosse AL, Burrows BT, Angulo RM, Conrad PR, Himes SM, Mathews N, et al. (2015): mGluR5 positive allosteric modulation and its effects on MK-801 induced set-shifting impairments in a rat operant delayed matching/non-matching-to-sample task. *Psychopharmacology*. 232:251-258.
11. Xi D, Li YC, Snyder MA, Gao RY, Adelman AE, Zhang W, et al. (2011): Group II metabotropic glutamate receptor agonist ameliorates MK801-induced dysfunction of NMDA receptors via the Akt/GSK-3beta pathway in adult rat prefrontal cortex. *Neuropsychopharmacology : official publication of the American College of Neuropsychopharmacology*. 36:1260-1274.
12. Jope RS, Johnson GV (2004): The glamour and gloom of glycogen synthase kinase-3. *Trends Biochem Sci*. 29:95-102.
13. Su P, Li S, Chen S, Lipina TV, Wang M, Lai TK, et al. (2014): A Dopamine D2 Receptor-DISC1 Protein Complex may Contribute to Antipsychotic-Like Effects. *Neuron*. 84:1302-1316.

14. Li Y-C, Gao W-J (2011): GSK-3[beta] activity and hyperdopamine-dependent behaviors. *Neuroscience & Biobehavioral Reviews*. 35:645-654.
15. Zheng P, Zhang XX, Bunney BS, Shi WX (1999): Opposite modulation of cortical N-methyl-D-aspartate receptor-mediated responses by low and high concentrations of dopamine. *Neuroscience*. 91:527-535.
16. Seamans JK, Durstewitz D, Christie BR, Stevens CF, Sejnowski TJ (2001): Dopamine D1/D5 receptor modulation of excitatory synaptic inputs to layer V prefrontal cortex neurons. *Proceedings of the National Academy of Sciences of the United States of America*. 98:301-306.
17. Li YC, Liu G, Hu JL, Gao WJ, Huang YQ (2010): Dopamine D(1) receptor-mediated enhancement of NMDA receptor trafficking requires rapid PKC-dependent synaptic insertion in the prefrontal neurons. *Journal of neurochemistry*. 114:62-73.
18. Ochs SM, Dorostkar MM (2015): Loss of neuronal GSK3beta reduces dendritic spine stability and attenuates excitatory synaptic transmission via beta-catenin. 20:482-489.
19. Khlghatyan J, Evstratova A, Chamberland S, Marakhovskaia A, Bahremand A, Toth K, et al. (2018): Mental Illnesses-Associated Fxr1 and Its Negative Regulator Gsk3beta Are Modulators of Anxiety and Glutamatergic Neurotransmission. *Front Mol Neurosci*. 11:119.
20. Chen P, Gu Z, Liu W, Yan Z (2007): Glycogen synthase kinase 3 regulates N-methyl-D-aspartate receptor channel trafficking and function in cortical neurons. *Molecular pharmacology*. 72:40-51.
21. Wei J, Liu W, Yan Z (2010): Regulation of AMPA receptor trafficking and function by glycogen synthase kinase 3. *Journal of Biological Chemistry*. 285:26369-26376.
22. Collingridge GL, Volianskis A, Bannister N, France G, Hanna L, Mercier M, et al. (2013): The NMDA receptor as a target for cognitive enhancement. *Neuropharmacology*. 64:13-26.
23. Peineau S, Taghibiglou C, Bradley C, Wong TP, Liu L, Lu J, et al. (2007): LTP inhibits LTD in the hippocampus via regulation of GSK3beta. *Neuron*. 53:703-717.
24. Zhu LQ, Wang SH, Liu D, Yin YY, Tian Q, Wang XC, et al. (2007): Activation of glycogen synthase kinase-3 inhibits long-term potentiation with synapse-associated impairments. *The Journal of neuroscience : the official journal of the Society for Neuroscience*. 27:12211-12220.
25. Malenka RC, Bear MF (2004): LTP and LTD: an embarrassment of riches. *Neuron*. 44:5-21.
26. NÃ¤gerl UV, Eberhorn N, Cambridge SB, Bonhoeffer T (2004): Bidirectional activity-dependent morphological plasticity in hippocampal neurons. *Neuron*. 44:759-767.
27. Okamoto K-I, Nagai T, Miyawaki A, Hayashi Y (2004): Rapid and persistent modulation of actin dynamics regulates postsynaptic reorganization underlying bidirectional plasticity. *Nature neuroscience*. 7:1104-1112.
28. Zhou Q, Homma KJ, Poo M-m (2004): Shrinkage of dendritic spines associated with long-term depression of hippocampal synapses. *Neuron*. 44:749-757.
29. Feldmeyer D (2012): Excitatory neuronal connectivity in the barrel cortex. *Frontiers in neuroanatomy*. 6:24.
30. Harris KD, Shepherd GM (2015): The neocortical circuit: themes and variations. *Nature neuroscience*. 18:170-181.
31. De Roo M, Klauser P, Garcia PM, Poglia L, Muller D (2008): Spine dynamics and synapse remodeling during LTP and memory processes. *Progress in brain research*. 169:199-207.
32. Glantz LA, Lewis DA (2000): Decreased dendritic spine density on prefrontal cortical pyramidal neurons in schizophrenia. *Arch Gen Psychiatry*. 57:65-73.

33. Glausier JR, Lewis DA (2013): Dendritic spine pathology in schizophrenia. *Neuroscience*. 251:90-107.
34. Garey L, Ong W, Patel T, Kanani M, Davis A, Mortimer A, et al. (1998): Reduced dendritic spine density on cerebral cortical pyramidal neurons in schizophrenia. *Journal of Neurology, Neurosurgery & Psychiatry*. 65:446-453.
35. Roberts AC, Diez-Garcia J, Rodriguiz RM, Lopez IP, Lujan R, Martinez-Turrillas R, et al. (2009): Downregulation of NR3A-containing NMDARs is required for synapse maturation and memory consolidation. *Neuron*. 63:342-356.
36. Snyder MA, Adelman AE, Gao WJ (2013): Gestational methylazoxymethanol exposure leads to NMDAR dysfunction in hippocampus during early development and lasting deficits in learning. *Neuropsychopharmacology : official publication of the American College of Neuropsychopharmacology*. 38:328-340.
37. Das S, Sasaki YF, Rothe T, Premkumar LS, Takasu M, Crandall JE, et al. (1998): Increased NMDA current and spine density in mice lacking the NMDA receptor subunit NR3A. *Nature*. 393:377-381.
38. Sasaki YF, Rothe T, Premkumar LS, Das S, Cui J, Talantova MV, et al. (2002): Characterization and comparison of the NR3A subunit of the NMDA receptor in recombinant systems and primary cortical neurons. *Journal of neurophysiology*. 87:2052-2063.
39. Yashiro K, Philpot BD (2008): Regulation of NMDA receptor subunit expression and its implications for LTD, LTP, and metaplasticity. *Neuropharmacology*. 55:1081-1094.
40. Paoletti P, Bellone C, Zhou Q (2013): NMDA receptor subunit diversity: impact on receptor properties, synaptic plasticity and disease. *Nature reviews Neuroscience*. 14:383-400.
41. Carta M, Srikumar BN, Gorlewicz A, Rebola N, Mulle C (2018): Activity-dependent control of NMDA receptor subunit composition at hippocampal mossy fibre synapses. *The Journal of physiology*. 596:703-716.
42. Cui Z, Feng R, Jacobs S, Duan Y, Wang H, Cao X, et al. (2013): Increased NR2A:NR2B ratio compresses long-term depression range and constrains long-term memory. *Sci Rep*. 3.
43. Peineau S, Taghibiglou C, Bradley C, Wong TP, Liu L, Lu J, et al. (2007): LTP inhibits LTD in the hippocampus via regulation of GSK3[beta]. *Neuron*. 53:703-717.
44. Peineau S, Bradley C, Taghibiglou C, Doherty A, Bortolotto ZA, Wang YT, et al. (2008): The role of GSK-3 in synaptic plasticity. *Br J Pharmacol*. 153:S428-S437.
45. Akbarian S, Sucher NJ, Bradley D, Tafazzoli A, Trinh D, Hetrick WP, et al. (1996): Selective alterations in gene expression for NMDA receptor subunits in prefrontal cortex of schizophrenics. *The Journal of neuroscience : the official journal of the Society for Neuroscience*. 16:19-30.
46. Jiang Y, Jakovcevski M, Bharadwaj R, Connor C, Schroeder FA, Lin CL, et al. (2010): Setdb1 histone methyltransferase regulates mood-related behaviors and expression of the NMDA receptor subunit NR2B. *J Neurosci*. 30:7152-7167.
47. Grayson DR, Guidotti A (2013): The dynamics of DNA methylation in schizophrenia and related psychiatric disorders. *Neuropsychopharmacology : official publication of the American College of Neuropsychopharmacology*. 38:138-166.
48. Grayson DR, Kundakovic M, Sharma RP (2010): Is there a future for histone deacetylase inhibitors in the pharmacotherapy of psychiatric disorders? *Mol Pharmacol*. 77:126-135.
49. Borrelli E, Nestler EJ, Allis CD, Sassone-Corsi P (2008): Decoding the epigenetic language of neuronal plasticity. *Neuron*. 60:961-974.

50. Day JJ, Sweatt JD (2011): Epigenetic modifications in neurons are essential for formation and storage of behavioral memory. *Neuropsychopharmacology : official publication of the American College of Neuropsychopharmacology*. 36:357-358.
51. Bharadwaj R, Peter Cyril J, Jiang Y, Roussos P, Vogel-Ciernia A, Shen EY, et al. (2014): Conserved higher-order chromatin regulates NMDA receptor gene expression and cognition. *Neuron*. 84:997-1008.
52. Gulchina Y, Xu SJ, Snyder MA, Elefant F, Gao WJ (2017): Epigenetic mechanisms underlying NMDA receptor hypofunction in the prefrontal cortex of juvenile animals in the MAM model for schizophrenia. *Journal of neurochemistry*. 143:320-333.
53. Gupta C, Kaur J, Tikoo K (2014): Regulation of MDA-MB-231 cell proliferation by GSK-3beta involves epigenetic modifications under high glucose conditions. *Experimental cell research*. 324:75-83.
54. Bardai FH, D'Mello SR (2011): Selective toxicity by HDAC3 in neurons: regulation by Akt and GSK3beta. *The Journal of neuroscience : the official journal of the Society for Neuroscience*. 31:1746-1751.
55. Cernotta N, Clocchiatti A, Florean C, Brancolini C (2011): Ubiquitin-dependent degradation of HDAC4, a new regulator of random cell motility. *Molecular biology of the cell*. 22:278-289.
56. Chen S, Owens GC, Makarenkova H, Edelman DB (2010): HDAC6 regulates mitochondrial transport in hippocampal neurons. *PloS one*. 5:e10848.
57. Fujita Y, Morinobu S, Takei S, Fuchikami M, Matsumoto T, Yamamoto S, et al. (2012): Vorinostat, a histone deacetylase inhibitor, facilitates fear extinction and enhances expression of the hippocampal NR2B-containing NMDA receptor gene. *Journal of psychiatric research*. 46:635-643.
58. Guan JS, Haggarty SJ, Giacometti E, Dannenberg JH, Joseph N, Gao J, et al. (2009): HDAC2 negatively regulates memory formation and synaptic plasticity. *Nature*. 459:55-60.
59. Kim MS, Akhtar MW, Adachi M, Mahgoub M, Bassel-Duby R, Kavalali ET, et al. (2012): An essential role for histone deacetylase 4 in synaptic plasticity and memory formation. *The Journal of neuroscience : the official journal of the Society for Neuroscience*. 32:10879-10886.
60. Xing B, Li YC, Gao WJ (2016): GSK3beta hyperactivity during an early critical period impairs prefrontal synaptic plasticity and induces lasting deficits in spine morphology and working memory. *Neuropsychopharmacology : official publication of the American College of Neuropsychopharmacology*. 41:3003-3015.
61. Nguyen T, Fan T, George SR, Perreault ML (2017): Disparate Effects of Lithium and a GSK-3 Inhibitor on Neuronal Oscillatory Activity in Prefrontal Cortex and Hippocampus. *Frontiers in aging neuroscience*. 9:434.
62. van der Vaart A, Meng X, Bowers MS, Batman AM, Aliev F, Farris SP, et al. (2018): Glycogen synthase kinase 3 beta regulates ethanol consumption and is a risk factor for alcohol dependence. *Neuropsychopharmacology : official publication of the American College of Neuropsychopharmacology*. 43:2521-2531.
63. Baddeley A (1998): Recent developments in working memory. *Current opinion in neurobiology*. 8:234-238.
64. Fuster JM (2000): Executive frontal functions. *Exp Brain Res*. 133:66-70.
65. Dias R, Robbins TW, Roberts AC (1997): Dissociable forms of inhibitory control within prefrontal cortex with an analog of the Wisconsin Card Sort Test: restriction to novel

situations and independence from "on-line" processing. *The Journal of neuroscience : the official journal of the Society for Neuroscience*. 17:9285-9297.
66. Stefani MR, Moghaddam B (2005): Systemic and prefrontal cortical NMDA receptor blockade differentially affect discrimination learning and set-shift ability in rats. *Behavioral neuroscience*. 119:420.
67. Ragozzino ME, Detrick S, Kesner RP (1999): Involvement of the prelimbic-infralimbic areas of the rodent prefrontal cortex in behavioral flexibility for place and response learning. *The Journal of neuroscience : the official journal of the Society for Neuroscience*. 19:4585-4594.
68. Birrell JM, Brown VJ (2000): Medial frontal cortex mediates perceptual attentional set shifting in the rat. *The Journal of neuroscience : the official journal of the Society for Neuroscience*. 20:4320-4324.
69. Stefani MR, Groth K, Moghaddam B (2003): Glutamate receptors in the rat medial prefrontal cortex regulate set-shifting ability. *Behav Neurosci*. 117:728-737.
70. Tamura M, Mukai J, Gordon JA, Gogos JA (2016): Developmental Inhibition of Gsk3 Rescues Behavioral and Neurophysiological Deficits in a Mouse Model of Schizophrenia Predisposition. *Neuron*. 89:1100-1109.
71. Block AE, Dhanji H, Thompson-Tardif SF, Floresco SB (2007): Thalamic–prefrontal cortical–ventral striatal circuitry mediates dissociable components of strategy set shifting. *Cerebral Cortex*. 17:1625-1636.
72. Ferguson BR, Gao WJ (2018): Thalamic Control of Cognition and Social Behavior Via Regulation of Gamma-Aminobutyric Acidergic Signaling and Excitation/Inhibition Balance in the Medial Prefrontal Cortex. *Biological psychiatry*. 83:657-669.
73. Nicholls RE, Alarcon JM, Malleret G, Carroll RC, Grody M, Vronskaya S, et al. (2008): Transgenic mice lacking NMDAR-dependent LTD exhibit deficits in behavioral flexibility. *Neuron*. 58:104-117.
74. Connor SA, Wang YT (2016): A Place at the Table: LTD as a Mediator of Memory Genesis. *The Neuroscientist : a review journal bringing neurobiology, neurology and psychiatry*. 22:359-371.
75. Dong Z, Bai Y, Wu X, Li H, Gong B, Howland JG, et al. (2013): Hippocampal long-term depression mediates spatial reversal learning in the Morris water maze. *Neuropharmacology*. 64:65-73.
76. Arguello PA, Gogos JA (2006): Modeling Madness in Mice: One Piece at a Time. *Neuron*. 52:179-196.
77. Tang W, Thevathasan JV, Lin Q, Lim KB, Kuroda K, Kaibuchi K, et al. (2016): Stimulation of Synaptic Vesicle Exocytosis by the Mental Disease Gene DISC1 is Mediated by N-Type Voltage-Gated Calcium Channels. *Frontiers in synaptic neuroscience*. 8:15.
78. Maher BJ, LoTurco JJ (2012): Disrupted-in-schizophrenia (DISC1) functions presynaptically at glutamatergic synapses. *PLoS ONE*. 7:e34053.